

## NRC Publications Archive Archives des publications du CNRC

### Subsonic aerodynamic coefficients of the SDM at angles of attack up to 90°

Huang, X. Z.; Beyers, M. E.

For the publisher's version, please access the DOI link below./ Pour consulter la version de l'éditeur, utilisez le lien DOI ci-dessous.

#### **Publisher's version / Version de l'éditeur:**

<https://doi.org/10.4224/40003398>

*Laboratory Technical Report (National Research Council of Canada. National Aeronautical Establishment. Unsteady Aerodynamics Laboratory); no. LTR-UA-93, 1990-01*

#### **NRC Publications Archive Record / Notice des Archives des publications du CNRC :**

<https://nrc-publications.canada.ca/eng/view/object/?id=442f8d60-9414-4460-8f2f-3a4e185cc052>

<https://publications-cnrc.canada.ca/fra/voir/objet/?id=442f8d60-9414-4460-8f2f-3a4e185cc052>

Access and use of this website and the material on it are subject to the Terms and Conditions set forth at

<https://nrc-publications.canada.ca/eng/copyright>

READ THESE TERMS AND CONDITIONS CAREFULLY BEFORE USING THIS WEBSITE.

L'accès à ce site Web et l'utilisation de son contenu sont assujettis aux conditions présentées dans le site

<https://publications-cnrc.canada.ca/fra/droits>

LISEZ CES CONDITIONS ATTENTIVEMENT AVANT D'UTILISER CE SITE WEB.

**Questions?** Contact the NRC Publications Archive team at

PublicationsArchive-ArchivesPublications@nrc-cnrc.gc.ca. If you wish to email the authors directly, please see the first page of the publication for their contact information.

**Vous avez des questions?** Nous pouvons vous aider. Pour communiquer directement avec un auteur, consultez la première page de la revue dans laquelle son article a été publié afin de trouver ses coordonnées. Si vous n'arrivez pas à les repérer, communiquez avec nous à PublicationsArchive-ArchivesPublications@nrc-cnrc.gc.ca.



National Research  
Council Canada

Conseil national  
de recherches Canada

UNLIMITED

UNCLASSIFIED

NATIONAL AERONAUTICAL  
ESTABLISHMENT

ÉTABLISSEMENT AÉRONAUTIQUE  
NATIONAL

PAGES 16  
PAGES \_\_\_\_\_

REPORT  
RAPPORT

REPORT LTR-UA-93  
RAPPORT \_\_\_\_\_

FIG. 28  
DIAG. \_\_\_\_\_

DATE January 1990  
DATE \_\_\_\_\_

LABORATORY / LABORATOIRE

TABLES 9  
TABLES \_\_\_\_\_

UNSTEADY AERODYNAMICS LABORATORY

LAB. ORDER  
COMM. LAB. \_\_\_\_\_

FILE 4012-8  
DOSSIER \_\_\_\_\_

FOR Internal  
POUR

REFERENCE  
RÉFÉRENCE

. LTR - UA-93

SUBSONIC AERODYNAMIC COEFFICIENTS OF THE  
SDM AT ANGLES OF ATTACK UP TO 90°

SUBMITTED BY K.J. Orlik-Ruckemann  
PRÉSENTÉ PAR \_\_\_\_\_  
LABORATORY HEAD  
CHEF DE LABORATOIRE

AUTHOR X.Z. Huang  
AUTEUR M.E. Beyers \_\_\_\_\_

APPROVED G.F. Marsters  
APPROUVÉ \_\_\_\_\_  
DIRECTOR  
DIRECTEUR

ANALYZED

6 14617365

## ABSTRACT

---

A test programme was undertaken to determine the subsonic aerodynamic coefficients of the Standard Dynamics Model at angles of attack up to  $90^\circ$  under conditions of minimal wall interference. Five component aerodynamic coefficients were measured at  $0^\circ$  and  $5^\circ$  sideslip, while a sideslip sweep was performed at high alpha. The onset of flow asymmetry was found to occur at near  $26^\circ$  angle of attack and asymmetrical flow conditions prevailed up to  $53^\circ$ . Large side-force asymmetries at angles of attack between  $53^\circ$  and  $69^\circ$  were attributed to asymmetrical vortex breakdown. The effects of sideslip angle on the aerodynamic characteristics were large and the lack of symmetry with respect to the zero sideslip condition at an angle of attack of  $36^\circ$  was attributed to the effects of forebody flow asymmetries. No definitive effects of wind speed/Reynolds number were observed. Measurable effects of sting diameter on the side-force and moment coefficients were observed at high alpha. Evidence of support-strut interference was found in the lateral-directional coefficients at angles of attack above  $69^\circ$ .

**CONTENTS**

	<b>Page</b>
ABSTRACT	i
NOMENCLATURE	iii
LIST OF TABLES	v
LIST OF ILLUSTRATIONS	vii
1.0 INTRODUCTION	1
2.0 TEST FACILITIES	1
2.1 Wind Tunnel and Model	1
2.2 Support System	2
2.3 Force Balance	2
3.0 TEST RESULTS AND DISCUSSION	4
3.1 Dependence on Angle of Attack and Velocity	4
3.2 Support Interference Effects	6
3.3 Effects of Angle of Sideslip	6
4.0 SUMMARY AND CONCLUSIONS	7
5.0 ACKNOWLEDGEMENT	8
6.0 REFERENCES	8
TABLES	
FIGURES	

## NOMENCLATURE

$b$	wingspan	m
$\bar{c}$	mean aerodynamic chord	m
$C_\ell$	rolling moment coefficient = $L/(qSb)$	
$C_m$	pitching moment coefficient = $M/(qSc)$	
$C_n$	yawing moment coefficient = $N/(qSb)$	
$C_Y$	side force coefficient = $Y/(qS)$	
$C_Z$	normal force coefficient = $Z/(qS)$	
$d$	body diameter at base	m
$d_r$	= $d_s/d$	
$d_s$	sting diameter	m
$K_1$	angular stiffness in pitch plane due to Z	deg/N
$K_2$	angular stiffness in pitch plane due to M	deg/N•m
$K_3$	angular stiffness in yaw plane due to Y	deg/N
$K_4$	angular stiffness in yaw plane due to N	deg/N•m
$l_s$	sting length	m
$\bar{L}, \bar{M}, \bar{N}$	rolling, pitching and yawing moment	N•m
$L$	rolling moment output of balance	mV
$M$	freestream Mach number	
$\bar{N}_1, \bar{N}_2$	forward and aft normal force output of balance	mV
$N_1, N_2$	forward and aft normal force components	N
$q$	freestream dynamic pressure	N/m <sup>2</sup>

$Re_c$	Reynolds number based on $c$	
$S$	reference area (wing area)	$m^2$
$V$	freestream velocity	$m/s$
$x,y,z$	body axes system	
$X_T, Y_T, Z_T$	tunnel-fixed axes system	
$X, Y$	axial and side force	$N$
$\bar{Y}_1, \bar{Y}_2$	forward and aft side force output of balance	$mV$
$Y_1, Y_2$	forward and aft side force components	$N$
$Z$	normal force	$N$
$Z_1, Z_2$	forward and aft normal force components	$N$
$\alpha$	angle of attack	deg
$\beta$	angle of sideslip	deg
$\Delta\alpha, \Delta\beta$	deflections due to aerodynamic load	deg
$\sigma$	aerodynamic angle of attack	deg
$\psi$	aerodynamic angle of bank	deg

**LIST OF TABLES****Table**

1	Test Matrix
2	Aerodynamic Coefficients at $V = 100$ m/s ( $\beta = 0^\circ$ , $d_r = 0.4$ )
3	Aerodynamic Coefficients at $V = 69$ m/s ( $\beta = 0^\circ$ , $d_r = 0.4$ )
4	Aerodynamic Coefficients at $\beta = 5^\circ$ ( $V = 100$ m/s, $d_r = 0.4$ )
5	Sideslip Effect ( $V = 100$ m/s, $\alpha = 36^\circ$ , $d_r = 0.4$ )
6	Sting Interference Effect ( $V = 100$ m/s, $\beta = 0^\circ$ ) (a) $d_r = 0.5$ , (b) $d_r = 0.6$ , (c) $d_r = 0.7$

**LIST OF ILLUSTRATIONS****Figure**

1	Standard Dynamics Model
2	Test Installation in Wind Tunnel
3	Balance Installation in Wind Tunnel
4	Support Geometry
5	Force System and Dimensions of Balance
6	Reference Systems
7	Normal Force at Two Velocities
8	Side Force at Two Velocities
9	Pitching Moment at Two Velocities
9(a)	Pitching Moment at Two Velocities
10	Rolling Moment at Two Velocities
11	Yawing Moment at Two Velocities
12	Sting Diameter Effect: Normal Force
13	Sting Diameter Effect: Side Force
14	Sting Diameter Effect: Pitching Moment
15	Sting Diameter Effect: Rolling Moment
16	Sting Diameter Effect: Yawing Moment
17	Sideslip Effect on Normal Force
18	Sideslip Effect on Side Force
19	Sideslip Effect on Pitching Moment

19(a)	Sideslip Effect on Pitching Moment
20	Sideslip Effect on Rolling Moment
21	Sideslip Effect on Yawing Moment
22	Normal Force vs Sideslip
23	Side Force vs Sideslip
24	Pitching Moment vs Sideslip
25	Rolling Moment vs Sideslip
26	Yawing Moment vs Sideslip

## 1.0 INTRODUCTION

Since its introduction at NAE in 1978<sup>(1)</sup>, the Standard Dynamics Model (SDM), a generic fighter aircraft configuration, has undergone extensive testing in several countries<sup>(2-7)</sup>. The direct, cross and cross-coupling derivatives have been determined at nonzero sideslip and angles of attack up to 40°. With the current emphasis on aircraft manoeuvring at high  $\alpha$  there is some interest in the SDM characteristics in the range up to  $\alpha = 90^\circ$ .

The NAE dynamic tests were conducted in the 0.40 m x 0.75 m Dynamics Wind Tunnel. Because of the large wingspan-to-tunnel-width ratio,  $b/w = 0.608$ , the measured subsonic aerodynamic data required relatively large wall corrections. Hence, to facilitate the analysis of these data, and as a first step towards extending the SDM data base to  $\alpha = 90^\circ$ , a series of static tests were conducted on the same model in the NAE 2 m x 3 m Low Speed Wind Tunnel (LSWT). Wind tunnel wall interference was minimal in these tests, where the wingspan-to-tunnel-width ratio was  $b/w = 0.076$ .

Five-component static aerodynamic loads were measured over the range  $0 < \alpha < 90^\circ$  and the effects of angle of sideslip, freestream speed and sting diameter were investigated. The test Reynolds numbers were  $Re_c = 0.39 \times 10^6$  and  $0.58 \times 10^6$ .

## 2.0 TEST FACILITIES

### 2.1 Wind Tunnel and Model

The experiments were conducted in the LSWT<sup>(8)</sup>. The test section measures 1.93 m high by 2.74 m wide and 4.57 m long at the balance centreline. The empty-tunnel maximum dynamic pressure is about 7182 N/m<sup>2</sup> (at 106.6 m/s) and the maximum useful dynamic pressure is about 5267 N/m<sup>2</sup> (at 91.4 m/s), corresponding to a Reynolds number of about  $6.56 \times 10^6/m$ . A turbulence level of 0.1%, a velocity variation of  $\pm 0.25\%$  and a  $\pm 0.5\%$  variation in total and static pressure coefficients were measured<sup>(8)</sup> at 27.4 m/s. A turbulence level of 0.25% was measured at 61 m/s.

The data acquisition and reduction procedures were implemented on a DEC PDP 11/70 minicomputer and two DEC LSI-11 processors were used as front-end devices to acquire the analogue and digital data.

An all-aluminum SDM having a wingspan of 0.2286 m was used in these tests. Salient details of the model geometry are given in Figure 1. The ratio of fuselage length to tunnel width was  $l/w = 0.129$  and the span-to-height ratio was  $b/h = 0.118$ . Wall interference was, therefore, expected to be negligible, even at high angles of attack.

## 2.2 Support System

The model was mounted on a slender sting attached to an elbow-shaped extension of one of the wind tunnel struts. The latter was enclosed in a fairing and mounted on the wind tunnel turntable as shown in Figures 2 to 4. The pitch axis was coincident with the turntable axis of rotation and arbitrary angles of attack could be set to an accuracy of  $\pm 0.1^\circ$ <sup>(9)</sup>. The ratio of sting length to model base diameter was about  $l_s/d = 3.5$  while sting diameter ratios in the range of  $0.4 < d_s/d < 0.7$  were available.

The roll orientation of the model relative to the balance was fixed while the roll position of the model-balance assembly was set by measurements taken from the orientation of the model. The total error in model roll angle due to the distributed set-up errors was within  $\pm 0.1^\circ$ . The sideslip angle was varied by changing the roll angle.

## 2.3 Force Balance

The model was tested on an internal six-component strain-gauge balance having an outside diameter of 19.05 mm. Forces are sensed directly at forward and aft locations and pitching and yawing moments obtained indirectly, while the rolling moment is measured directly.

The balance design loads are<sup>(10)</sup>

Forward Normal Force	(N <sub>1</sub> )	445 (N)
Aft Normal Force	(N <sub>2</sub> )	445 (N)
Forward Side Force	(Y <sub>1</sub> )	133 (N)
Aft Side Force	(Y <sub>2</sub> )	133 (N)
Rolling Moment	(L)	5.65 (N•m)
Axial Force	(X)	133 (N)

In this experiment, the axial force component was not used.

The sensitivity of the balance was approximately 0.6 millivolt/volt input at the full-load condition. A 6-volt power supply was used. The transient temperature errors did not exceed 1 percent of the full-load output<sup>(10)</sup>.

The force and moment system and balance dimensions are illustrated in Figure 5 and the reference systems are shown in Figure 6. Static check calibrations were performed in the laboratory<sup>(11)</sup> and in situ in the wind tunnel. This confirmed the results of an earlier calibration. The following balance and deflection equations were used:

$$\begin{aligned}Z_1 &= 61.18 \bar{N}_1 + 0.4442 \bar{N}_2 - 0.1135 \bar{Y}_1 \\Z_2 &= 2.283 \bar{N}_1 + 54.49 \bar{N}_2 - 0.0253 \bar{Y}_1 - 0.1316 \bar{Y}_2 \\Y_1 &= 0.1196 \bar{N}_1 - 0.0239 \bar{N}_2 + 16.11 \bar{Y}_1 + 0.2643 \bar{Y}_2 \\Y_2 &= -0.1851 \bar{N}_1 + 0.03068 \bar{N}_2 + 0.1202 \bar{Y}_1 + 18.40 \bar{Y}_2 \\L &= -0.9096 L\end{aligned}\tag{1}$$

$$\begin{aligned}\Delta\alpha &= K_1Z + K_2M = 0.0032Z + 0.0266M \\ \Delta\beta &= K_3Y + K_4N = -0.0032Y - 0.0314N\end{aligned}\tag{2}$$

### 3.0 TEST RESULTS AND DISCUSSION

The test conditions and objectives are summarized in the test matrix given in Table 1. The nominal angle of attack increment was  $2^\circ$  but in the  $\beta = 5^\circ$  tests  $\sigma$  and  $\psi$  were varied to yield  $2.5^\circ$  steps in  $\alpha$ .

Following standard procedures the dynamic pressure was corrected for solid blockage and corrections were applied to the angle of attack to account for upwash caused by the tunnel walls. As noted earlier, these wall effects were miniscule. Wake blockage was also small, the correction to  $q$  being on the order of 1% at  $\alpha = 90^\circ$ , and was not corrected for.

The data obtained are presented in this Chapter, and a possible aerodynamic interpretation of the trends observed is given, based on the widely accepted understanding of vortex flows. Since the force and moment measurements were not accompanied by pressure measurements or flow visualization studies, the interpretation given is, of course, of a speculative nature.

#### 3.1 Dependence on Angle of Attack and Velocity

The aerodynamic data are presented in Figures 7 to 11, as functions of  $\alpha$  for two freestream velocities. The numerical data appear in Tables 2 and 3.

From Figure 7 it is clear that, due to incremental strake lift, the normal force curve is extended dramatically beyond the wing-alone stall angle, which, for the flat surfaces of the SDM, is expected to be in the vicinity of  $\alpha = 18^\circ$ . Also, the aerodynamic characteristics in the range  $\alpha = 18^\circ$  to  $22^\circ$  have been found to be consistent with the strake vortex burst occurring over the trailing edge<sup>(7)</sup>. The resulting loss of lift is seen as the reason for the kink in the  $C_z$  curve near  $\alpha = 18^\circ$ . As  $\alpha$  is further increased the vortex-induced lift increases up to perhaps  $\alpha = 45^\circ$ , where the vortex burst occurs near the leading edge.

The pitching moment curve is linear up to  $\alpha \simeq 15^\circ$  except at very small  $\alpha$ , where both  $C_z$  and  $C_m$  are small (Figs. 9 and 9(a)). It appears that separation on the horizontal stabilizer is

delayed by downwash from the wing so that the normal force slope of the stabilizer is kept at relatively high values due to the effectively lower angle of attack. Thus, when the wing  $C_{Z\alpha}$  is reduced by tip stalling above  $\alpha = 18^\circ$ , a stabilizing pitching moment results. The favourable effect of the wing downwash is maintained up to about  $30^\circ$ , above which the longitudinal stability is lost. At very high  $\alpha$  ( $\alpha > 54^\circ$ ),  $C_{m\alpha}$  is again stabilizing by virtue of the increasing separation drag of the stabilizer.

The directional static data at  $\beta = 0$  (Fig. 11) show that the asymmetry starts near  $\alpha \approx 26^\circ$ , which is nearly double the nose apex angle and is, therefore, probably caused by the asymmetrical forebody vortex effects on the strake vortex system. Combining Figure 8 with Figure 11, it will be noticed that in the range  $26^\circ < \alpha < 55^\circ$ , the centre of pressure of the resultant side force is located forward of the reference centre for one of the two repeat runs and aft of it for the other. At higher  $\alpha$ ,  $C_Y$  (Fig. 8) and  $C_n$  (Fig. 11) reverse direction, within the ranges  $40^\circ \leq \alpha \leq 68^\circ$  and  $55^\circ \leq \alpha \leq 65^\circ$ , respectively, apparently as the vortex breakdown asymmetry on the wing flips from one side to the other.

The effect on the normal force of changing the velocity from 100 to 69 m/s, corresponding to Reynolds numbers of  $0.57 \times 10^6$  and  $0.39 \times 10^6$ , respectively, is negligible as might be expected for this configuration (see Fig. 7). In the case of the pitching moment, depicted in Figures 9 and 9(a), the velocity/Reynolds-number effects were, in general, also small, but measurable differences were observed at  $\alpha \geq 30^\circ$  (Fig. 9(a)). Opposite side force directions were recorded in the range  $40^\circ \leq \alpha \leq 65^\circ$ , for two runs at the same velocity,  $V_\infty = 100$  m/s (see Fig. 8), while the data at 69 m/s were similar to one of these runs. This shows that the differences between the  $C_Y$  data at  $V = 100$  and 69 m/s are not due to velocity/Reynolds-number effects. The effects at high  $\alpha$  of vortex asymmetry due to nose micro-asymmetries provide a more likely explanation. The rolling moments are very small at  $\beta = 0$ , as seen in Figure 10, and the differences between the two data sets at  $V = 100$  m/s and that at  $V = 69$  m/s are largely within the experimental uncertainty (note that the scale of  $C_l$  is exaggerated in Fig. 10).

### 3.2 Support Interference Effects

The results obtained with sting diameters of between  $d_r = 0.4$  and  $0.7$  are shown in Figures 12 to 16 together with Table 6. In the range  $65^\circ \leq \alpha \leq 77^\circ$  the data obtained with  $d_r = 0.6$  and  $0.7$  were invalid owing to an electrical problem and are consequently omitted. Figures 12 and 14 show that sting diameter effects on the normal force and pitching moment are negligible over the entire  $\alpha$  range. This is also the case for the side force and yawing moment at low  $\alpha$  (see Figs. 13 and 16). However, some discrepancies between the different curves appear at high  $\alpha$ , in the presence of asymmetrical vortex shedding. At angles of attack above  $28^\circ$ ,  $C_Y$  is initially slightly larger for the large sting diameters (Fig. 13) but there is no readily apparent correlation with  $d_r$  at  $\alpha > 40^\circ$ . In the range  $36^\circ < \alpha < 53^\circ$ , the somewhat larger  $C_n$  values seem to result from the increase of  $d_r$  to  $0.6$  or  $0.7$  (Fig. 16). For the rolling moment (Fig. 15), the differences between data for different  $d_r$  values are small compared with the experimental uncertainty (see also Fig. 10). The negative average values of  $C_l$  at low  $\alpha$  ( $\alpha \leq 10^\circ$ ) may be partly due to freestream flow asymmetries.

The small, nonzero average values of the yawing moment and side force at angles of attack approaching  $90^\circ$ , in Figures 11 and 16 and Figures 8 and 13, respectively, were probably caused by local flow acceleration between the strut and tunnel walls. The flow acceleration effects (and deflections) naturally increase in magnitude as the strut moves upstream with increasing  $\alpha$  (Fig. 2). However, the actual magnitudes of the measured side force and yawing moment increments may be affected by the uncertainty due to balance interactions at high  $\alpha$ ; the  $Z_1$  and  $Z_2$  interactions on the side force had been observed to be nonlinear<sup>(10)</sup>, resulting in some error when used in Equation (1). Moreover, the small, finite average values of  $C_l$  at low  $\alpha$  ( $\alpha \leq 20^\circ$ ) could be the result of flow deflections produced by the strut (Figs. 10 and 15).

### 3.3 Effects of Angle of Sideslip

The effects of sideslip angle was investigated over the range of angle of attack for two values of sideslip,  $\beta = 0$  and  $5^\circ$  (Figs. 17 to 21), and at fixed angle of attack,  $\alpha = 36^\circ$ , for a range of  $\beta$  values (Figs. 22 to 26). The numerical data appear in Tables 2, 4 and 5.

The normal force is unaffected by  $\beta$  at low  $\alpha$  but decreases slightly at  $\beta = 5^\circ$  as  $\alpha$  is increased above  $45^\circ$ ; this difference disappears near  $\alpha = 60^\circ$  with diminishing vortex lift (Fig. 17). When  $\alpha$  exceeds about  $18^\circ$  the magnitude of the side force (Fig. 18) decreases and the yawing moment goes from positive to negative, probably as the result of increased separation around the tail fin. This effect seems to be amplified by the asymmetry of strake vortices at higher  $\alpha$ , when the vortex closest to the body approaches the vertical stabilizer. When the angle of attack continues to increase, the inboard vortex core crosses the centreline plane, possibly near  $\alpha = 45^\circ$ ; this could explain the increased weathercock stability at angles up to  $\alpha = 61^\circ$ , where the flow is totally separated (see Fig. 21).

In the  $\beta$ -sweep experiment at  $\alpha = 36^\circ$ , the side force and yawing moment trends for small  $\beta$  are approximately linear within the experimental uncertainty, as expected (see Figs. 23 and 26 respectively). The dependence of normal force (Fig. 22) and pitching moment (Fig. 24) on sideslip is not symmetrical as would be the case at low  $\alpha$ . Since the asymmetry of the strake vortex system will be determined by the interaction with the forebody vortices, the direction of the asymmetrical loads will be determined by forebody micro-asymmetries. The values of certain coefficients obtained at  $\alpha = 36^\circ$  and  $\beta = 0^\circ$  and  $5^\circ$  are in agreement with their counterparts in the fixed- $\beta$  experiment as can be seen, for instance, in comparing Figures 21 and 26.

The experimental data were compared with published results from AEDC<sup>(3)</sup> at  $\beta = 0$  and a higher Reynolds number. The results of the interfacility comparison will appear in a separate publication.

#### 4.0 SUMMARY AND CONCLUSIONS

Static aerodynamic coefficients were obtained for the SDM at angles of attack up to  $90^\circ$ . Effects of sideslip angle, wind speed and sting diameter were investigated under conditions of very low wall interference. Good repeatability of the measurements was demonstrated, except for cases where vortex asymmetry was clearly bistable.

- (a) The aerodynamic characteristics of the SDM are consistent with asymmetrical vortex shedding becoming dominant in the range  $26^\circ < \alpha < 53^\circ$  and asymmetrical vortex breakdown occurring on the wing at higher  $\alpha$  ( $53^\circ \leq \alpha \leq 69^\circ$ ).

- (b) The lateral-directional coefficients exhibited nonlinear dependence on angle of sideslip as well as angle of attack. The variations with  $\beta$  of the longitudinal-aerodynamic and rolling-moment coefficients are asymmetrical at  $\alpha = 36^\circ$ .
- (c) There was no distinct effect of velocity/Reynolds number for wind speeds between 69 m/s and 100 m/s.
- (d) Sting diameter effects were negligible at low angles of attack. Small but measurable effects of  $d_r$  on the side-force and moment coefficients were observed in the range  $28^\circ < \alpha < 53^\circ$ .

## 5.0 ACKNOWLEDGEMENT

The authors wish to acknowledge the contribution of the Low Speed Aerodynamics Laboratory in providing the necessary personnel support and wind-tunnel time, and to express their appreciation to Mr. E. Peter for his dedicated support in this project.

## 6.0 REFERENCES

1. Beyers, M.E., Moulton, B.E., "Stability Derivatives Due to Oscillations in Roll for the Standard Dynamics Model at Mach 0.6", NRC, NAE LTR-UA-64, Jan. 1983.
2. Beyers, M.E., "Subsonic Roll Oscillation Experiments on the Standard Dynamics Model", AIAA Paper No. 83-2134, Aug. 1983.
3. Coulter, S.M., Marquart, E.J., "Dynamic Stability Tests of the Standard Dynamics Model Utilizing the New 1500-lb Balance Mechanisms", AEDC-TSR-81-P11, Feb. 1981.
4. Coulter, S.M., Marquart, E.J., "Cross and Cross-Coupling Derivative Measurements on the Standard Dynamics Model at AEDC", AIAA Paper No. 82-0596, March 1982.
5. Schmidt, E., "Standard Dynamics Model Experiments with the DFVLR/AVA Transonic Derivative Balance", AGARD-CP-386-21, Nov. 1985.
6. Torngren, L., "Dynamic Pitch and Yaw Derivative of the Standard Dynamics Model", FFA TN 1985-5, Nov. 1985.
7. Beyers, M.E., "SDM Pitch-and-Yaw-Axis Stability Derivatives", AIAA 85-1827, Aug. 1985.

8. Brown, T.R., "Description of the 6-ft x 9-ft Low Speed Wind Tunnel", NRC, NAE LTR-LA-285, Nov. 1986.
9. Hansen, K., "Installation of Models in the 6-ft x 9-ft Low Speed Wind Tunnel", NRC, NAE LTR-LA-286, Aug. 1986.
10. LaBerge, J.G., "Calibration of TASK Corporation 6-Component Strain Gauge Balance", NRC, NAE HSAL-M-129, Jan. 1959.
11. Huang, X.Z., "The Recent Calibration of TASK Balance", NRC, NAE LM-UA-218, May 1988.



TABLE 2 - AERODYNAMIC COEFFICIENTS AT V = 100 m/s ( $\beta = 0^\circ$ ,  $d_r = 0.4$ )

ALPHA	BETA	CL	CM	CN	CY	CZ	V(M/S)
0.09	0.01	0.0000	-0.0008	0.0000	0.0000	0.0000	101.26
2.14	0.01	-0.0014	-0.0291	0.0000	0.0006	0.1753	101.19
4.18	0.01	-0.0026	-0.0195	-0.0007	0.0021	0.3147	101.15
6.25	0.01	-0.0029	-0.0095	-0.0010	0.0018	0.4439	101.20
8.30	0.01	-0.0028	0.0130	-0.0013	0.0027	0.5708	101.21
10.35	0.01	-0.0014	0.0297	-0.0006	0.0005	0.6744	101.24
12.41	0.01	0.0001	0.0498	-0.0007	0.0008	0.7872	101.30
14.45	0.01	-0.0009	0.0802	-0.0006	-0.0005	0.9201	101.36
16.51	0.01	0.0002	0.0832	-0.0007	0.0001	1.0940	101.36
18.59	0.01	0.0020	0.0719	-0.0009	0.0007	1.1956	101.32
20.56	0.01	0.0012	0.0621	-0.0016	0.0021	1.2310	101.37
22.58	0.01	0.0003	0.0525	-0.0029	0.0043	1.2982	101.37
24.61	0.01	-0.0002	0.0435	-0.0020	0.0013	1.4024	101.40
26.65	0.01	0.0005	0.0380	-0.0037	0.0025	1.5027	101.41
28.68	0.01	-0.0004	0.0345	-0.0041	0.0003	1.6032	101.47
30.71	0.01	0.0006	0.0315	-0.0061	0.0033	1.6919	101.48
32.78	0.01	0.0017	0.0321	-0.0078	0.0056	1.7759	101.61
34.82	0.01	0.0013	0.0273	-0.0079	0.0049	1.8534	101.47
36.83	0.01	0.0008	0.0318	-0.0076	0.0037	1.9416	101.50
38.84	0.01	0.0001	0.0314	-0.0064	0.0044	2.0194	101.58
40.87	0.01	-0.0012	0.0353	-0.0061	0.0079	2.1009	101.53
42.93	0.01	-0.0026	0.0447	-0.0048	0.0129	2.1543	101.61
44.91	0.01	-0.0032	0.0554	-0.0051	0.0135	2.1973	101.67
46.92	0.01	-0.0031	0.0669	-0.0060	0.0117	2.2248	101.68
48.93	0.01	-0.0034	0.0831	-0.0055	0.0115	2.2390	101.65
50.92	0.01	-0.0013	0.0822	-0.0063	-0.0020	2.2226	101.74
52.92	0.01	-0.0027	0.0851	-0.0096	0.0057	2.2133	101.76
54.92	0.01	-0.0016	0.0789	-0.0062	0.0021	2.1916	101.81
56.91	0.01	-0.0036	0.0691	-0.0155	0.0278	2.1823	101.82
58.93	0.01	-0.0038	0.0374	-0.0210	0.0330	2.1561	101.84
60.86	0.01	-0.0030	0.0070	-0.0172	0.0215	2.1569	101.78
62.84	0.01	0.0000	-0.0443	0.0085	-0.0159	2.1420	101.82
64.82	0.01	-0.0021	-0.1324	-0.0048	-0.0019	2.0923	101.88
66.77	0.02	-0.0018	-0.2218	-0.0163	-0.0007	2.0294	101.86
68.76	0.01	-0.0006	-0.2552	-0.0073	0.0071	2.0243	101.91
70.74	0.01	-0.0007	-0.3207	-0.0060	0.0083	2.0086	101.91
72.78	0.01	-0.0008	-0.3515	-0.0063	0.0093	2.0070	101.94
74.71	0.01	-0.0008	-0.3753	-0.0067	0.0077	2.0066	102.00
76.69	0.01	-0.0007	-0.3967	-0.0070	0.0093	1.9982	101.96
78.70	0.01	-0.0008	-0.4210	-0.0069	0.0123	2.0028	102.04
80.68	0.01	-0.0001	-0.4481	-0.0059	0.0088	2.0006	102.01
82.66	0.01	-0.0004	-0.4650	-0.0061	0.0123	2.0080	102.02
84.65	0.01	-0.0008	-0.4953	-0.0069	0.0157	2.0072	102.01
86.63	0.01	-0.0007	-0.5211	-0.0055	0.0124	2.0120	102.08
88.64	0.01	-0.0006	-0.5476	-0.0066	0.0152	2.0092	102.09

TABLE 2 - CONTINUED (REPEAT TEST)

ALPHA	BETA	CL	CM	CN	CY	CZ	V(M/S)
0.10	0.00	0.0000	0.0002	0.0000	0.0000	0.0000	102.99
2.15	0.00	-0.0037	-0.0257	-0.0011	0.0035	0.1694	102.89
4.20	0.00	-0.0043	-0.0181	-0.0005	0.0007	0.3076	102.87
6.26	0.00	-0.0051	-0.0068	-0.0010	0.0020	0.4412	103.00
8.32	0.00	-0.0053	0.0124	-0.0008	0.0013	0.5619	102.90
10.34	0.00	-0.0046	0.0289	-0.0015	0.0041	0.6685	102.99
12.39	0.00	-0.0025	0.0498	-0.0012	0.0025	0.7899	102.94
14.46	0.01	-0.0016	0.0768	-0.0003	-0.0015	0.9281	102.90
16.52	0.01	-0.0016	0.0786	-0.0002	-0.0035	1.1009	102.96
18.58	0.01	0.0005	0.0689	-0.0002	-0.0052	1.2013	102.99
20.56	0.01	0.0002	0.0603	-0.0013	-0.0011	1.2393	102.95
22.58	0.01	-0.0003	0.0507	-0.0019	-0.0004	1.3040	102.98
24.61	0.01	-0.0011	0.0407	-0.0020	-0.0015	1.4005	102.98
26.64	0.01	-0.0005	0.0356	-0.0033	0.0004	1.5037	103.01
28.69	0.01	0.0000	0.0308	-0.0049	0.0013	1.5954	103.03
30.73	0.01	-0.0006	0.0295	-0.0060	0.0013	1.6858	102.99
32.76	0.01	0.0017	0.0278	-0.0086	0.0034	1.7705	103.02
34.78	0.01	0.0010	0.0299	-0.0072	-0.0006	1.8585	103.13
36.80	0.01	0.0002	0.0330	-0.0066	0.0012	1.9554	103.01
38.85	0.01	-0.0004	0.0291	-0.0074	0.0001	2.0210	103.11
40.87	0.01	-0.0006	0.0379	-0.0070	-0.0010	2.1001	103.12
42.90	0.01	-0.0021	0.0445	-0.0062	-0.0022	2.1585	103.06
44.95	0.01	-0.0017	0.0567	-0.0069	-0.0040	2.2055	103.11
46.91	0.01	-0.0014	0.0663	-0.0077	-0.0121	2.2323	103.10
48.94	0.01	-0.0007	0.0772	-0.0071	-0.0154	2.2288	103.19
50.91	0.01	-0.0012	0.0819	-0.0050	-0.0106	2.2261	103.17
52.92	0.02	-0.0015	0.0721	-0.0053	-0.0198	2.1863	103.24
54.91	0.01	0.0016	0.0741	0.0032	-0.0357	2.1897	103.19
56.90	0.01	0.0009	0.0625	0.0081	-0.0339	2.1751	103.20
58.89	0.01	-0.0002	0.0401	0.0081	-0.0268	2.1625	103.29
60.88	0.01	-0.0003	0.0056	0.0078	-0.0204	2.1576	103.35
62.87	0.00	-0.0006	-0.0562	0.0093	-0.0161	2.1316	103.27
64.85	0.01	-0.0022	-0.1392	-0.0053	-0.0033	2.0884	103.32
66.77	0.01	-0.0022	-0.2316	-0.0119	-0.0025	2.0221	103.32
68.75	0.00	-0.0021	-0.2635	-0.0052	0.0112	2.0304	104.16
70.72	0.00	-0.0019	-0.3315	-0.0042	0.0134	2.0129	104.16
72.71	0.00	-0.0011	-0.3584	-0.0035	0.0115	2.0111	104.20
74.71	0.00	-0.0013	-0.3799	-0.0046	0.0157	2.0093	104.18
76.70	0.00	-0.0013	-0.4001	-0.0033	0.0144	2.0097	104.22
78.70	0.00	-0.0011	-0.4270	-0.0028	0.0155	2.0177	104.25
80.68	0.00	-0.0011	-0.4409	-0.0019	0.0175	2.0034	104.18
82.68	0.00	-0.0013	-0.4721	-0.0008	0.0222	2.0170	104.26
84.66	0.00	-0.0008	-0.4958	0.0005	0.0222	2.0138	104.24
86.70	-0.01	-0.0009	-0.5163	0.0020	0.0241	2.0118	104.23
88.64	-0.01	-0.0007	-0.5442	0.0035	0.0276	2.0238	104.25

TABLE 3 - AERODYNAMIC COEFFICIENTS AT V = 69 m/s ( $\beta = 0^\circ$ ,  $d_r = 0.4$ )

ALPHA	BETA	CL	CM	CN	CY	CZ	V(M/S)
0.09	0.00	0.0000	-0.0049	0.0000	0.0000	0.0000	70.10
2.14	0.00	-0.0012	-0.0288	0.0000	-0.0006	0.1967	70.12
4.13	0.00	-0.0007	-0.0209	-0.0008	0.0013	0.3208	70.16
6.17	0.00	-0.0013	-0.0123	-0.0003	-0.0020	0.4567	70.18
8.20	0.00	-0.0017	0.0054	-0.0003	-0.0010	0.5772	70.22
10.27	0.00	-0.0005	0.0211	0.0001	-0.0037	0.6869	70.20
12.24	0.00	-0.0011	0.0412	-0.0008	0.0014	0.8168	70.20
14.27	0.00	-0.0004	0.0691	0.0001	-0.0029	0.9173	70.29
16.29	0.00	-0.0008	0.0739	-0.0002	-0.0041	1.0808	70.20
18.32	0.00	0.0017	0.0647	-0.0003	-0.0022	1.1983	70.24
20.36	0.00	0.0011	0.0540	-0.0009	-0.0029	1.2454	70.22
22.36	0.00	0.0011	0.0466	-0.0012	-0.0018	1.3088	70.23
24.40	0.00	0.0009	0.0468	-0.0012	-0.0017	1.4053	70.21
26.38	0.00	0.0005	0.0421	-0.0026	0.0006	1.4976	70.15
28.43	0.00	0.0008	0.0403	-0.0049	0.0032	1.5906	70.12
30.42	0.00	0.0012	0.0424	-0.0056	0.0045	1.6905	70.17
32.44	0.01	0.0010	0.0452	-0.0068	-0.0006	1.7830	70.21
34.44	0.01	0.0013	0.0436	-0.0070	0.0010	1.8663	70.20
36.48	0.01	0.0010	0.0462	-0.0067	-0.0017	1.9570	70.23
38.47	0.01	0.0008	0.0463	-0.0062	-0.0017	2.0350	70.16
40.50	0.01	-0.0001	0.0491	-0.0056	-0.0031	2.1144	70.18
42.50	0.01	-0.0010	0.0554	-0.0051	-0.0021	2.1766	70.20
44.53	0.01	-0.0022	0.0660	-0.0036	-0.0045	2.2281	70.18
46.55	0.00	-0.0042	0.0784	-0.0025	0.0035	2.2588	70.21
48.52	0.00	-0.0045	0.0961	-0.0026	0.0054	2.2663	70.17
50.54	0.00	-0.0041	0.1056	-0.0042	0.0065	2.2741	70.18
52.55	0.00	-0.0048	0.1118	-0.0075	0.0081	2.2631	70.18
54.52	0.01	-0.0054	0.1070	-0.0136	0.0166	2.2354	70.20
56.52	0.01	-0.0066	0.0881	-0.0215	0.0341	2.2096	70.24
58.51	0.01	-0.0047	0.0626	-0.0220	0.0204	2.1832	70.23
60.50	0.01	-0.0044	-0.0041	-0.0288	0.0393	2.1396	70.22
62.48	0.01	-0.0031	-0.0397	-0.0168	0.0203	2.1272	70.17
64.46	0.00	-0.0009	-0.0652	-0.0007	0.0028	2.1494	70.23
66.46	0.00	-0.0003	-0.1949	-0.0029	0.0091	2.0446	70.24
68.43	0.00	-0.0005	-0.2264	-0.0048	0.0126	2.0352	70.26
70.47	0.00	-0.0004	-0.3157	-0.0062	0.0083	2.0078	70.25
72.41	0.00	-0.0005	-0.3419	-0.0051	0.0053	2.0058	70.24
74.39	0.00	-0.0002	-0.3654	-0.0043	0.0043	1.9943	70.25
76.39	0.00	-0.0001	-0.3928	-0.0050	0.0082	1.9945	70.26
78.39	0.00	-0.0001	-0.4170	-0.0054	0.0099	2.0017	70.28
80.38	0.00	-0.0002	-0.4427	-0.0060	0.0107	1.9903	70.23
82.37	0.00	0.0002	-0.4681	-0.0057	0.0100	2.0017	70.28
84.37	0.00	0.0000	-0.4925	-0.0052	0.0095	2.0008	70.29
86.35	0.00	0.0002	-0.5119	-0.0054	0.0092	1.9898	70.25
88.36	0.00	0.0004	-0.5422	-0.0056	0.0104	1.9943	70.23



TABLE 4 - AERODYNAMIC COEFFICIENTS AT  $\beta = 5^\circ$  ( $V = 100$  m/s,  $d_r = 0.4$ )

ALPHA	BETA	CL	CM	CN	CY	CZ	V(M/S)
0.09	5.02	-0.0043	0.0112	0.0144	-0.0766	-0.0285	103.00
5.23	5.03	-0.0116	-0.0037	0.0145	-0.1023	0.3619	102.98
7.81	5.02	-0.0118	0.0051	0.0144	-0.1071	0.5204	102.95
10.35	5.02	-0.0111	0.0240	0.0124	-0.1010	0.6583	102.90
12.91	5.03	-0.0073	0.0452	0.0125	-0.1102	0.7996	102.85
15.48	5.01	-0.0142	0.0645	0.0128	-0.1170	0.9817	102.80
18.03	5.01	-0.0020	0.0528	0.0069	-0.0972	1.1114	102.76
20.56	5.01	-0.0032	0.0439	0.0008	-0.0779	1.2235	102.68
23.10	4.98	-0.0045	0.0425	-0.0029	-0.0647	1.3108	102.62
25.61	5.05	-0.0015	0.0283	-0.0098	-0.0552	1.4000	102.65
28.16	5.05	0.0037	0.0222	-0.0202	-0.0455	1.5103	102.54
30.72	5.01	0.0048	0.0218	-0.0250	-0.0423	1.6454	102.48
33.26	5.03	0.0031	0.0251	-0.0263	-0.0473	1.7762	102.45
35.80	5.06	0.0022	0.0332	-0.0287	-0.0445	1.9019	102.39
38.34	5.04	0.0014	0.0443	-0.0309	-0.0347	2.0083	102.32
40.86	5.03	-0.0039	0.0274	-0.0222	-0.0374	2.0538	102.51
43.39	5.03	-0.0016	0.0396	-0.0227	-0.0481	2.1212	102.42
45.92	5.01	-0.0002	0.0486	-0.0225	-0.0596	2.1588	102.41
50.89	5.06	0.0047	0.0514	-0.0045	-0.1295	2.1274	102.22
55.87	5.00	0.0013	0.0309	0.0136	-0.1576	2.1112	102.08
60.87	4.99	-0.0049	-0.0518	0.0068	-0.1299	2.1260	102.25
65.79	5.02	-0.0071	-0.1646	-0.0109	-0.1115	2.0396	102.16
68.24	5.12	-0.0074	-0.2474	-0.0200	-0.0956	2.0028	102.10
70.73	5.00	-0.0064	-0.3152	-0.0164	-0.0932	1.9941	102.16
73.21	5.08	-0.0072	-0.3587	-0.0149	-0.0949	1.9832	102.20
75.70	5.00	-0.0069	-0.3858	-0.0123	-0.0973	1.9806	102.08
78.21	5.06	-0.0076	-0.4129	-0.0121	-0.0952	1.9779	102.14
80.68	5.10	-0.0075	-0.4489	-0.0112	-0.0952	1.9955	102.11
83.17	5.02	-0.0078	-0.4739	-0.0109	-0.0895	1.9999	102.19
85.66	5.05	-0.0068	-0.5036	-0.0079	-0.0958	1.9896	102.27
88.15	5.06	-0.0064	-0.5361	-0.0080	-0.0984	1.9909	102.21
90.63	5.07	-0.0065	-0.5632	-0.0074	-0.1041	1.9842	102.14



TABLE 5 – SIDESLIP EFFECT ( $V = 100$  m/s,  $\alpha = 36^\circ$ ,  $d_r = 0.4$ )

ALPHA	BETA	CL	CM	CN	CY	CZ	V(M/S)
36.81	-7.11	0.0035	0.0322	0.0229	0.0737	1.9230	101.77
36.80	-5.95	0.0012	0.0378	0.0188	0.0595	1.9337	101.92
36.81	-4.74	0.0007	0.0342	0.0134	0.0426	1.9271	101.72
36.80	-3.56	0.0021	0.0323	0.0067	0.0304	1.9254	101.75
36.80	-2.38	0.0044	0.0293	0.0003	0.0330	1.9094	101.69
36.80	-1.16	0.0052	0.0291	-0.0037	0.0207	1.9037	101.71
36.78	0.00	0.0057	0.0267	-0.0069	0.0098	1.8976	101.72
36.78	1.21	0.0045	0.0254	-0.0091	-0.0034	1.9021	101.78
36.80	2.36	0.0018	0.0247	-0.0111	-0.0177	1.8994	101.90
36.79	3.54	0.0006	0.0175	-0.0155	-0.0291	1.8934	101.96
36.79	4.76	-0.0021	0.0159	-0.0212	-0.0365	1.8873	102.15
36.79	5.96	-0.0008	0.0146	-0.0280	-0.0470	1.8844	102.05
36.78	7.16	-0.0028	0.0129	-0.0351	-0.0601	1.8790	102.09



TABLE 6 - STING INTERFERENCE EFFECT ( $V = 100$  m/s,  $\beta = 0^\circ$ )  
(a)  $d_r = 0.5$

ALPHA	BETA	CL	CM	CN	CY	CZ	V(M/S)
0.10	0.00	0.0000	-0.0026	0.0000	0.0000	0.0000	102.30
2.14	0.00	-0.0017	-0.0315	-0.0007	0.0005	0.1723	102.07
4.19	0.00	0.0002	-0.0230	-0.0007	0.0029	0.3238	102.09
6.25	0.00	-0.0011	-0.0153	-0.0008	0.0031	0.4574	102.13
8.36	0.00	-0.0011	0.0063	-0.0003	-0.0012	0.5788	102.10
10.35	0.00	0.0002	0.0227	-0.0002	-0.0008	0.6819	102.06
12.43	0.00	0.0023	0.0505	-0.0003	-0.0008	0.8040	102.26
14.47	0.00	0.0000	0.0778	-0.0005	-0.0008	0.9200	102.16
16.56	0.00	0.0007	0.0771	-0.0011	0.0026	1.1029	102.11
18.54	0.00	0.0029	0.0678	-0.0012	0.0024	1.1947	102.15
20.55	0.01	0.0022	0.0604	-0.0015	0.0005	1.2310	102.19
22.58	0.00	0.0010	0.0486	-0.0029	0.0060	1.2963	102.24
24.59	0.00	-0.0001	0.0417	-0.0022	0.0046	1.4008	102.18
26.67	0.01	0.0012	0.0334	-0.0038	0.0042	1.5046	102.29
28.68	0.01	0.0011	0.0315	-0.0049	0.0032	1.5992	102.27
30.76	0.01	0.0019	0.0272	-0.0056	0.0026	1.6882	102.24
32.72	0.01	0.0031	0.0287	-0.0073	0.0022	1.7676	102.32
34.78	0.01	0.0022	0.0253	-0.0076	0.0010	1.8551	102.28
36.81	0.01	0.0015	0.0259	-0.0072	-0.0008	1.9349	102.32
38.87	0.01	0.0007	0.0288	-0.0064	-0.0030	2.0167	102.33
40.85	0.01	-0.0001	0.0274	-0.0064	0.0010	2.0777	102.34
42.93	0.01	-0.0019	0.0431	-0.0039	0.0022	2.1560	102.33
44.92	0.01	-0.0015	0.0504	-0.0053	-0.0009	2.1940	102.39
46.95	0.01	-0.0015	0.0643	-0.0055	-0.0054	2.2198	102.44
48.91	0.01	-0.0013	0.0745	-0.0050	-0.0027	2.2237	102.44
50.96	0.01	0.0000	0.0818	-0.0044	-0.0151	2.2199	102.46
52.96	0.01	-0.0028	0.0897	-0.0073	0.0028	2.2190	102.48
54.99	0.01	-0.0009	0.0816	-0.0076	-0.0075	2.1967	102.46
56.92	0.01	-0.0016	0.0619	-0.0119	0.0121	2.1676	102.56
58.93	0.01	-0.0003	0.0370	0.0032	-0.0184	2.1549	102.47
60.86	0.00	0.0007	-0.0031	0.0064	-0.0134	2.1458	102.52
62.88	0.00	0.0011	-0.0550	0.0120	-0.0244	2.1405	102.53
64.76	0.01	-0.0017	-0.1549	-0.0163	0.0117	2.0576	102.56
66.78	0.02	-0.0010	-0.2279	-0.0141	-0.0016	2.0348	102.58
68.81	0.01	-0.0002	-0.2466	-0.0064	0.0019	2.0429	102.64
70.77	0.01	0.0003	-0.3193	-0.0049	0.0015	2.0155	121.87
72.86	0.01	0.0004	-0.3570	-0.0054	0.0037	2.0140	102.72
74.69	0.01	0.0005	-0.3816	-0.0047	0.0005	2.0030	102.74
76.71	0.01	0.0011	-0.4107	-0.0046	0.0013	2.0180	102.70
78.72	0.01	0.0007	-0.4307	-0.0049	0.0019	2.0131	102.76
80.72	0.01	0.0009	-0.4548	-0.0058	0.0047	2.0140	102.74
82.66	0.01	0.0002	-0.4835	-0.0066	0.0082	2.0226	102.75
84.65	0.01	0.0004	-0.5047	-0.0063	0.0075	2.0143	102.81
86.64	0.01	0.0006	-0.5268	-0.0061	0.0073	2.0104	101.56
88.64	0.01	0.0001	-0.5551	-0.0051	0.0070	2.0083	102.84

TABLE 6 - CONTINUED (b)  $d_r = 0.6$

ALPHA	BETA	CL	CM	CN	CY	CZ	V(M/S)
0.09	0.01	0.0000	-0.0038	0.0000	0.0000	0.0000	102.50
2.14	0.01	-0.0020	-0.0335	-0.0008	0.0022	0.1773	102.36
4.20	0.01	-0.0018	-0.0236	-0.0007	0.0014	0.3243	102.45
6.24	0.01	-0.0024	-0.0150	-0.0009	0.0016	0.4530	102.50
8.30	0.01	-0.0020	0.0059	-0.0008	0.0020	0.5756	102.46
10.36	0.01	-0.0009	0.0242	-0.0006	0.0019	0.6789	102.46
12.43	0.01	0.0006	0.0493	-0.0005	0.0007	0.7978	102.46
14.44	0.01	-0.0007	-0.0763	-0.0011	0.0020	0.9153	102.47
16.54	0.01	-0.0006	0.0774	-0.0012	0.0025	1.0931	102.50
18.55	0.01	0.0015	0.0657	-0.0013	0.0023	1.1918	102.53
20.56	0.01	0.0005	0.0588	-0.0020	0.0029	1.2310	102.57
22.58	0.01	0.0004	0.0488	-0.0029	0.0062	1.2963	102.57
24.62	0.01	-0.0004	0.0418	-0.0034	0.0079	1.3940	102.58
26.66	0.01	0.0002	0.0327	-0.0041	0.0079	1.4971	102.65
28.67	0.01	-0.0003	0.0286	-0.0048	0.0061	1.5868	102.62
30.76	0.01	0.0002	0.0287	-0.0066	0.0106	1.6922	102.66
32.78	0.01	0.0014	0.0297	-0.0082	0.0130	1.7725	102.68
34.78	0.01	0.0006	0.0280	-0.0081	0.0117	1.8613	102.63
36.81	0.01	0.0009	0.0291	-0.0090	0.0118	1.9457	102.69
38.84	0.01	0.0004	0.0322	-0.0087	0.0112	2.0281	102.73
40.87	0.01	-0.0008	0.0351	-0.0088	0.0142	2.1015	102.68
42.91	0.01	-0.0010	0.0446	-0.0086	0.0085	2.1655	102.72
44.91	0.01	-0.0015	0.0574	-0.0081	0.0079	2.2074	102.73
46.93	0.01	-0.0007	0.0670	-0.0089	0.0061	2.2277	102.75
48.95	0.01	-0.0009	0.0720	-0.0075	0.0027	2.2273	102.83
50.92	0.01	-0.0019	0.0830	-0.0076	0.0097	2.2418	102.89
52.91	0.01	-0.0005	0.0818	-0.0059	0.0014	2.2262	102.82
54.91	0.01	0.0018	0.0710	-0.0003	-0.0130	2.1934	102.87
56.90	0.01	0.0005	0.0530	0.0038	-0.0207	2.1704	102.93
58.87	0.01	0.0000	0.0308	0.0070	-0.0176	2.1626	102.92
60.89	0.00	-0.0005	-0.0075	0.0072	-0.0045	2.1585	102.89
62.84	0.00	-0.0005	-0.0584	0.0124	-0.0135	2.1541	102.97
76.70	0.00	-0.0011	-0.4128	-0.0057	0.0159	2.0057	103.16
78.71	0.00	-0.0008	-0.4410	-0.0046	0.0132	2.0038	103.16
80.72	0.00	-0.0016	-0.4679	-0.0063	0.0204	2.0168	103.08
82.67	0.00	-0.0013	-0.4913	-0.0068	0.0200	2.0201	103.10
84.70	0.00	-0.0003	-0.5125	-0.0060	0.0167	2.0153	103.08
86.65	0.00	-0.0012	-0.5386	-0.0068	0.0216	2.0180	103.24
88.64	0.00	-0.0006	-0.5630	-0.0071	0.0215	2.0160	103.19

TABLE 6 - CONTINUED (c)  $d_r = 0.7$

ALPHA	BETA	CL	CM	CN	CY	CZ	V(M/S)
0.08	0.00	0.0000	-0.0008	0.0000	0.0000	0.0000	102.96
2.14	0.00	-0.0015	-0.0327	-0.0003	0.0002	0.1723	102.66
4.17	0.00	-0.0012	-0.0239	-0.0010	0.0032	0.3116	102.67
6.25	0.00	-0.0010	-0.0110	-0.0006	0.0010	0.4526	102.67
8.30	0.00	-0.0012	0.0077	-0.0010	0.0035	0.5658	102.63
10.32	0.00	0.0013	0.0285	-0.0007	0.0020	0.6692	102.68
12.40	0.00	0.0019	0.0497	-0.0005	-0.0004	0.7865	102.69
14.42	0.00	-0.0009	0.0758	-0.0016	0.0031	0.9175	102.79
16.52	0.01	-0.0007	0.0775	-0.0009	-0.0009	1.0925	102.67
18.77	0.01	0.0014	0.0651	-0.0016	0.0017	1.2027	102.66
20.61	0.00	0.0012	0.0590	-0.0029	0.0049	1.2320	102.76
22.62	0.01	-0.0003	0.0465	-0.0028	0.0040	1.2949	102.89
24.58	0.00	-0.0005	0.0358	-0.0030	0.0069	1.3899	102.77
26.65	0.00	-0.0006	0.0322	-0.0042	0.0088	1.4993	102.81
28.69	0.01	-0.0006	0.0243	-0.0049	0.0082	1.6008	102.76
30.82	0.01	0.0010	0.0255	-0.0073	0.0102	1.6988	102.84
32.76	0.01	0.0011	0.0248	-0.0079	0.0085	1.7740	102.81
34.76	0.01	0.0013	0.0276	-0.0079	0.0065	1.8612	112.79
36.81	0.01	0.0016	0.0253	-0.0086	0.0051	1.9475	102.98
38.84	0.01	0.0004	0.0240	-0.0079	0.0020	2.0259	102.83
40.92	0.01	-0.0004	0.0229	-0.0081	0.0022	2.0842	102.92
42.89	0.01	-0.0020	0.0412	-0.0058	0.0056	2.1687	102.92
44.93	0.01	-0.0027	0.0471	-0.0063	0.0019	2.2052	102.92
46.93	0.01	-0.0024	0.0622	-0.0076	-0.0003	2.2320	102.93
48.96	0.01	-0.0019	0.0698	-0.0071	-0.0030	2.2325	102.97
50.93	0.01	-0.0018	0.0719	-0.0063	-0.0051	2.2288	102.96
53.00	0.01	-0.0034	0.0786	-0.0083	0.0044	2.2369	103.04
54.93	0.01	-0.0026	0.0699	-0.0065	0.0048	2.2132	103.01
56.90	0.01	-0.0035	0.0559	-0.0118	0.0196	2.1933	103.09
58.90	0.01	-0.0023	0.0305	-0.0086	0.0136	2.1907	103.12
60.87	0.01	-0.0012	-0.0011	-0.0023	-0.0012	2.1841	103.11
62.86	0.00	-0.0010	-0.0557	0.0119	-0.0188	2.1787	103.16
76.70	0.01	-0.0007	-0.4182	-0.0071	0.0113	2.0074	103.21
78.73	0.00	-0.0007	-0.4440	-0.0071	0.0145	2.0070	103.20
80.69	0.01	-0.0008	-0.4699	-0.0065	0.0105	2.0165	103.24
82.67	0.01	0.0000	-0.4899	-0.0063	0.0106	2.0138	103.21
84.68	0.01	-0.0009	-0.5216	-0.0064	0.0120	2.0231	103.20
86.63	0.00	-0.0008	-0.5466	-0.0071	0.0155	2.0265	103.25
88.67	0.00	-0.0011	-0.5664	-0.0022	0.0215	2.0106	103.30



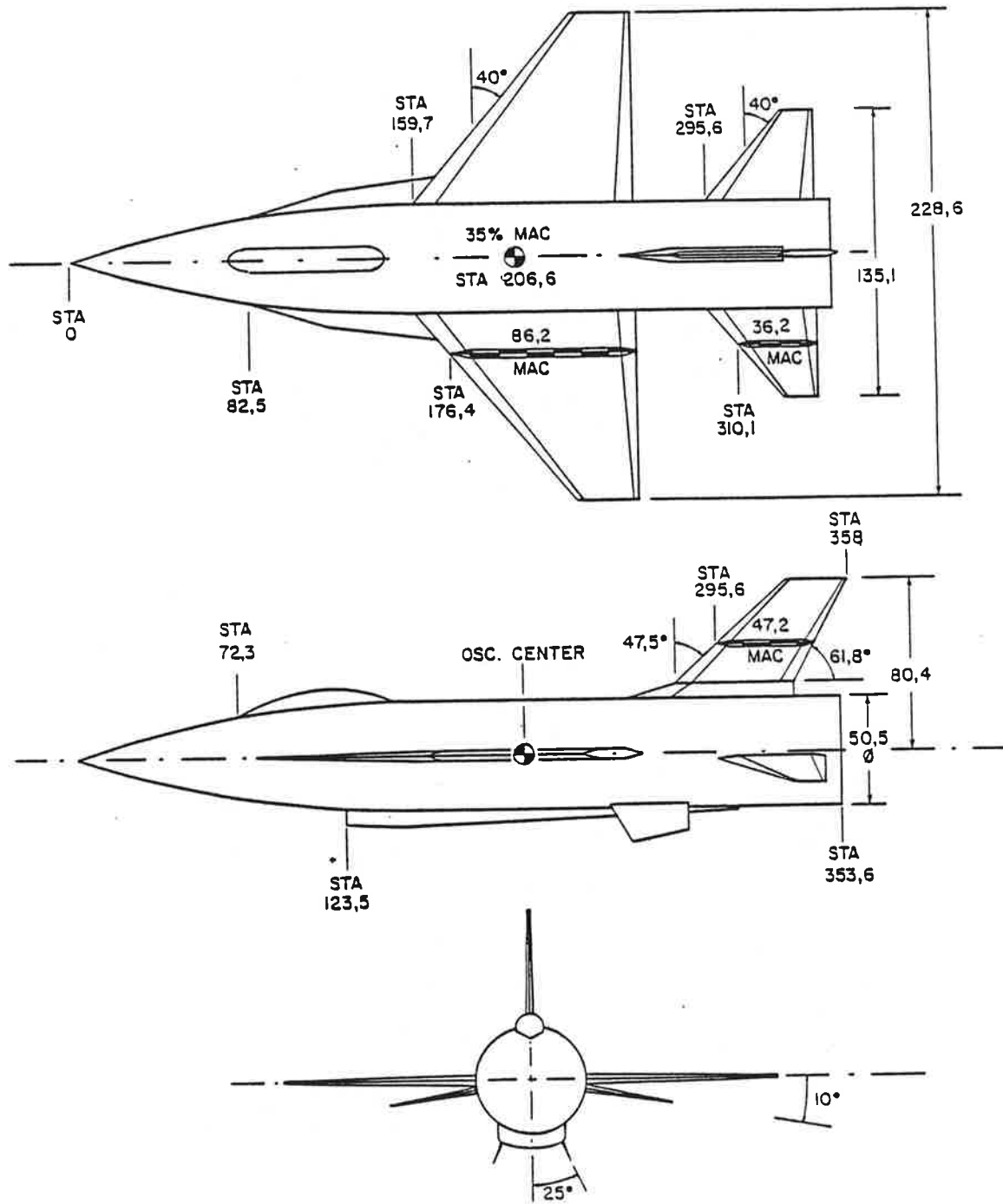


FIG. 1: GEOMETRICAL DETAILS OF THE STANDARD DYNAMICS MODEL

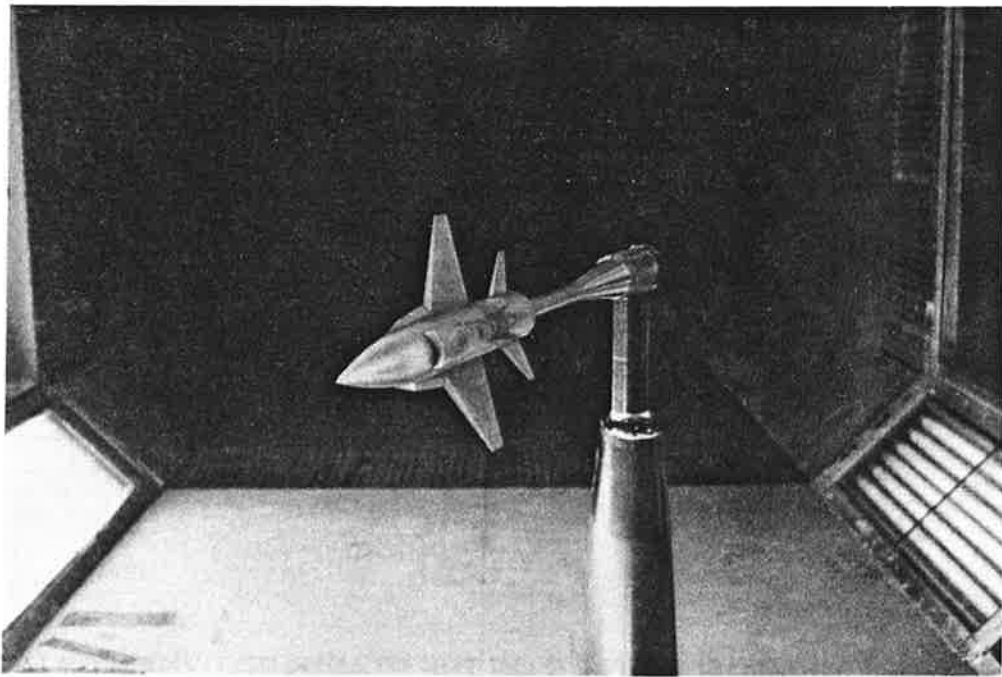
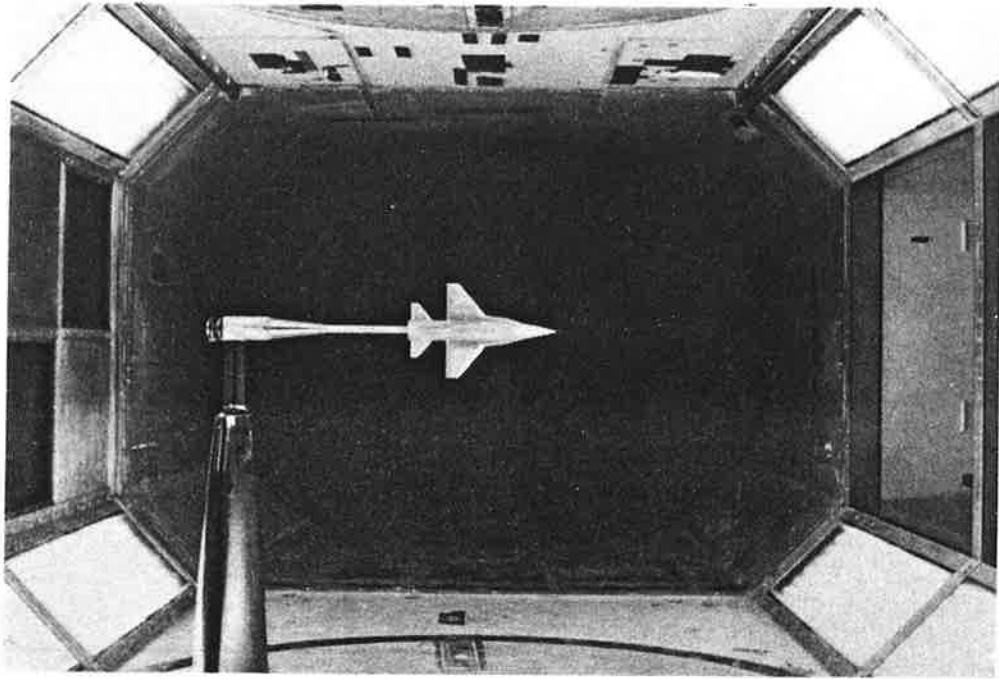


FIG. 2: TEST INSTALLATION IN WIND TUNNEL

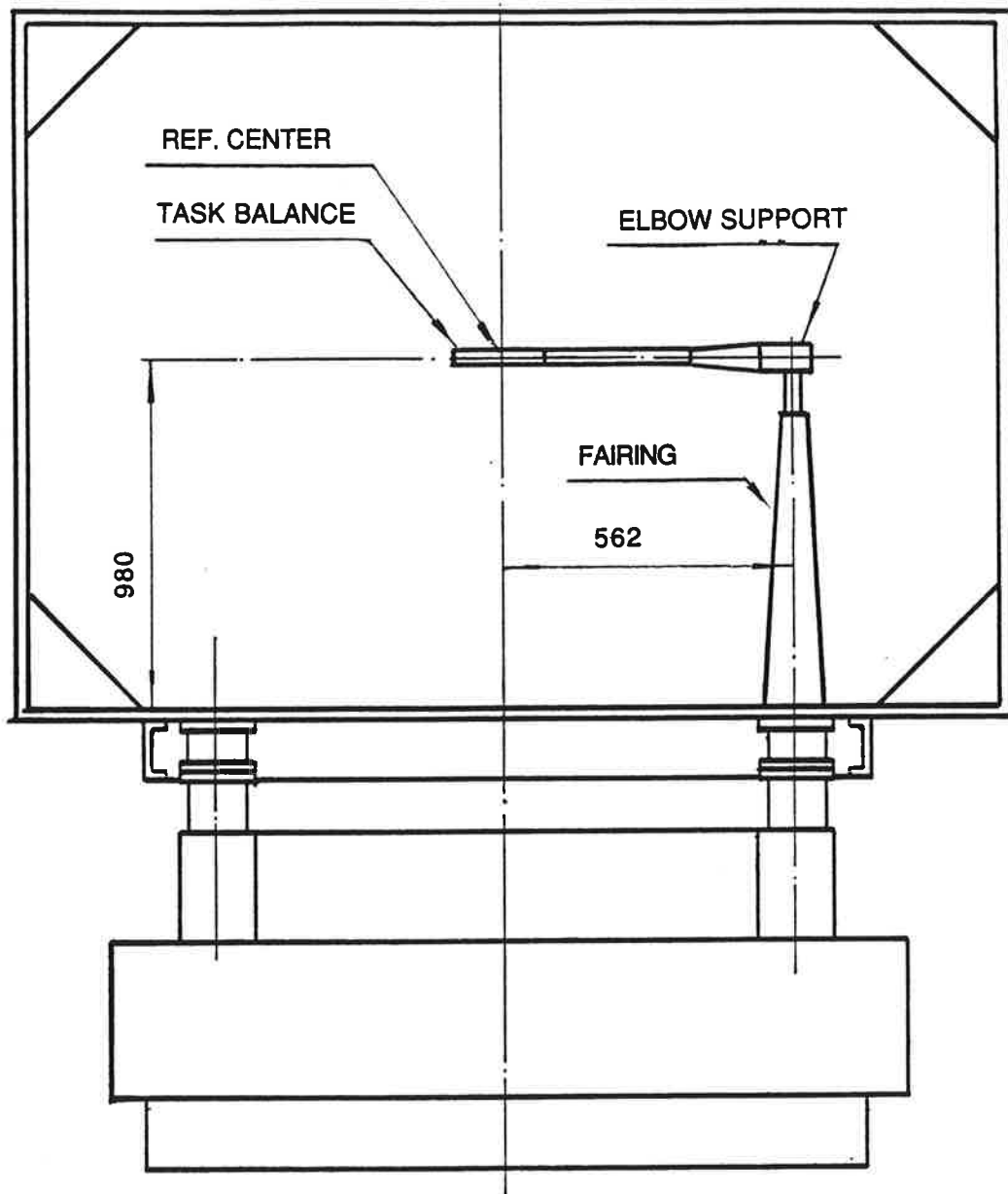


FIG. 3: BALANCE INSTALLATION IN WIND TUNNEL

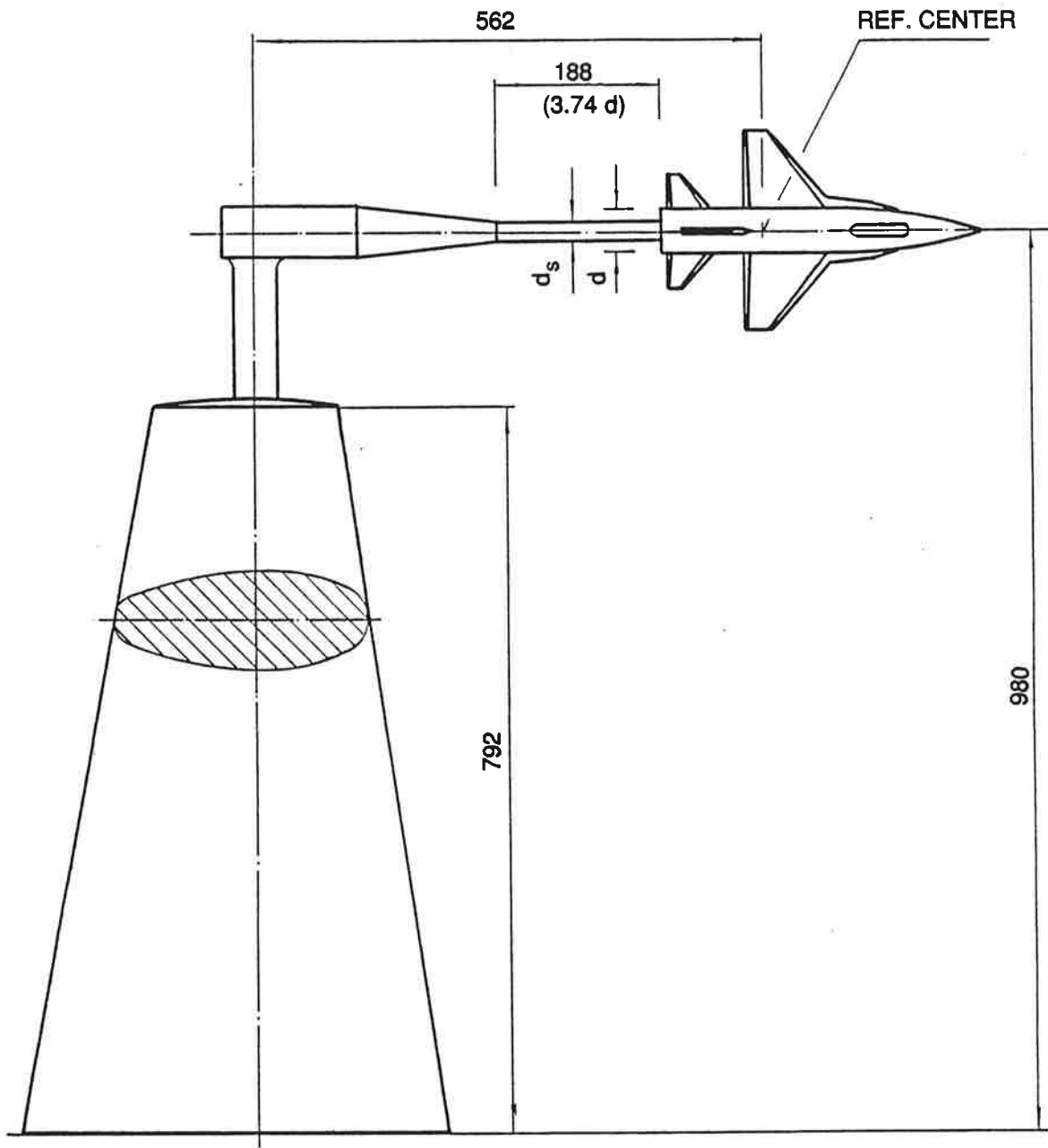
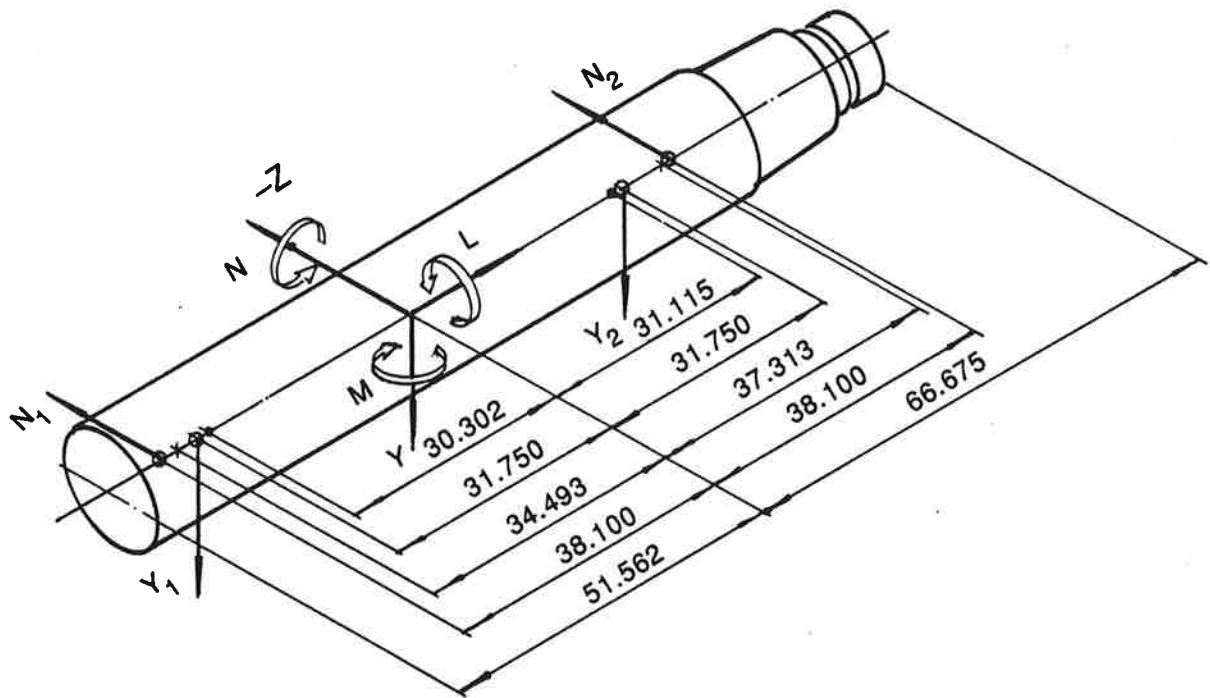


FIG. 4: SUPPORT GEOMETRY



- \* PITCH BRIDGE CENTER
- YAW BRIDGE CENTER
- FORCE CENTER

ARROWS ON FORCES AND MOMENTS POINT IN POSITIVE SENSE  
 ALL DIMENSIONS IN mm

FIG. 5: FORCE SYSTEM AND DIMENSIONS OF BALANCE

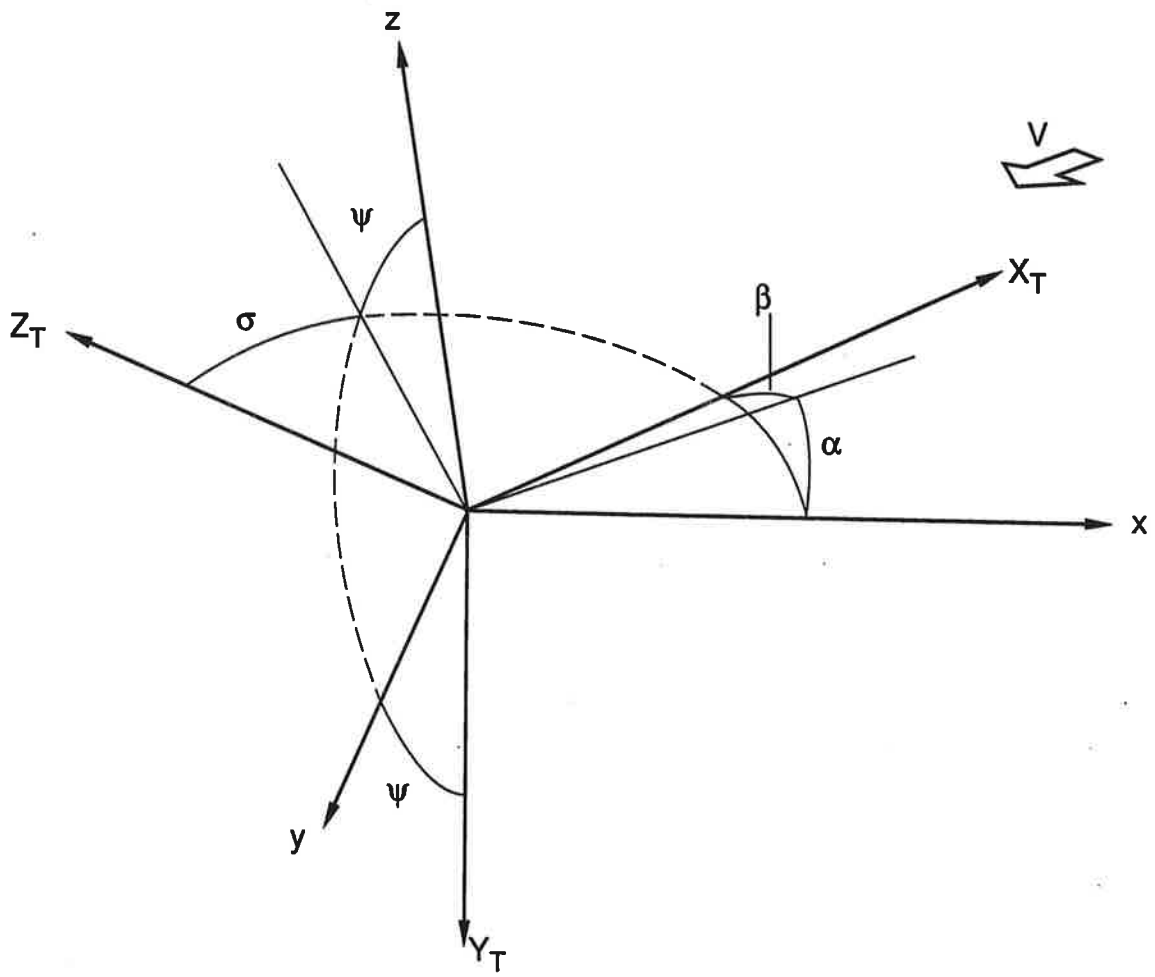


FIG. 6: REFERENCE SYSTEMS

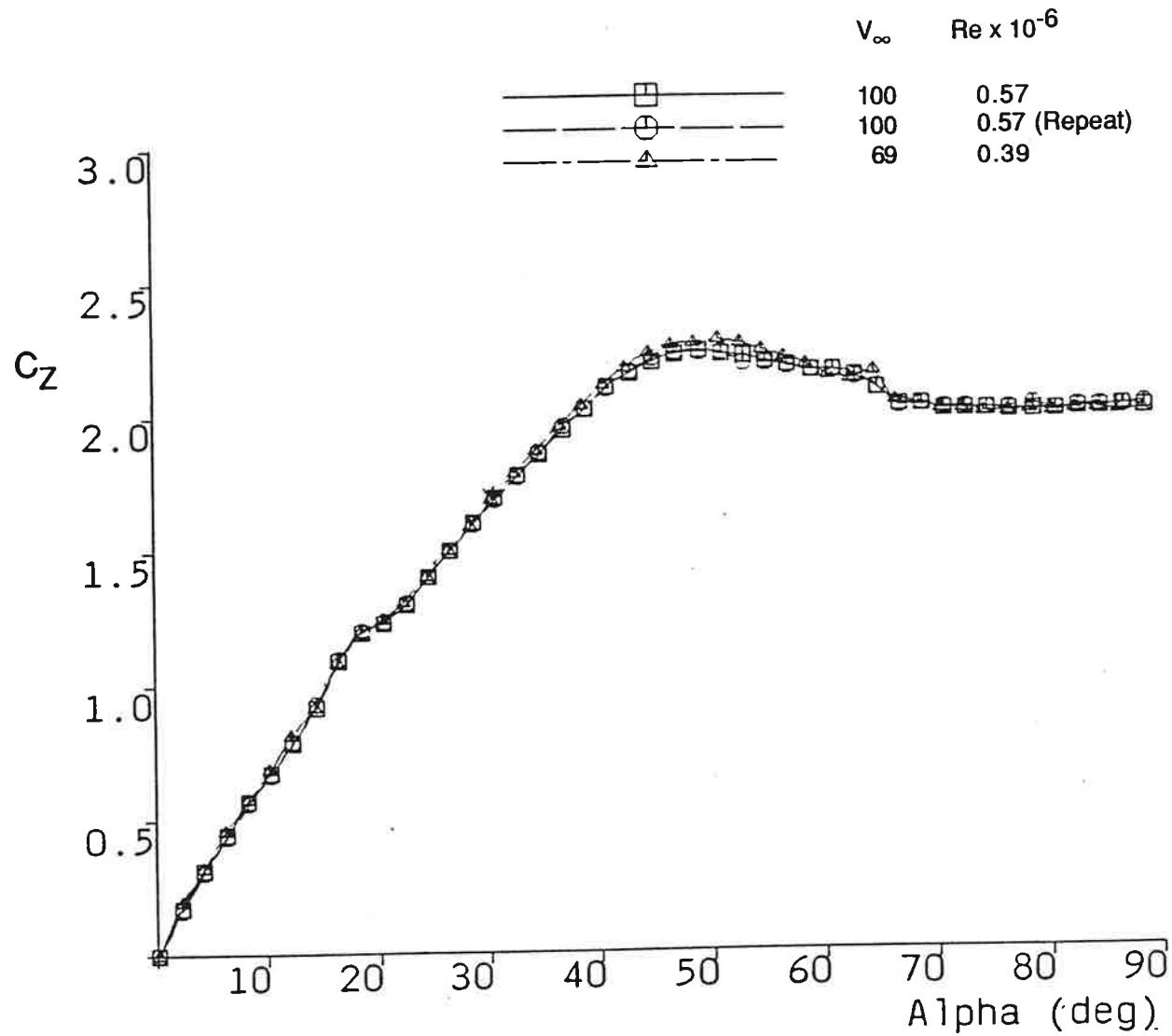


FIG. 7: NORMAL FORCE AT TWO VELOCITIES

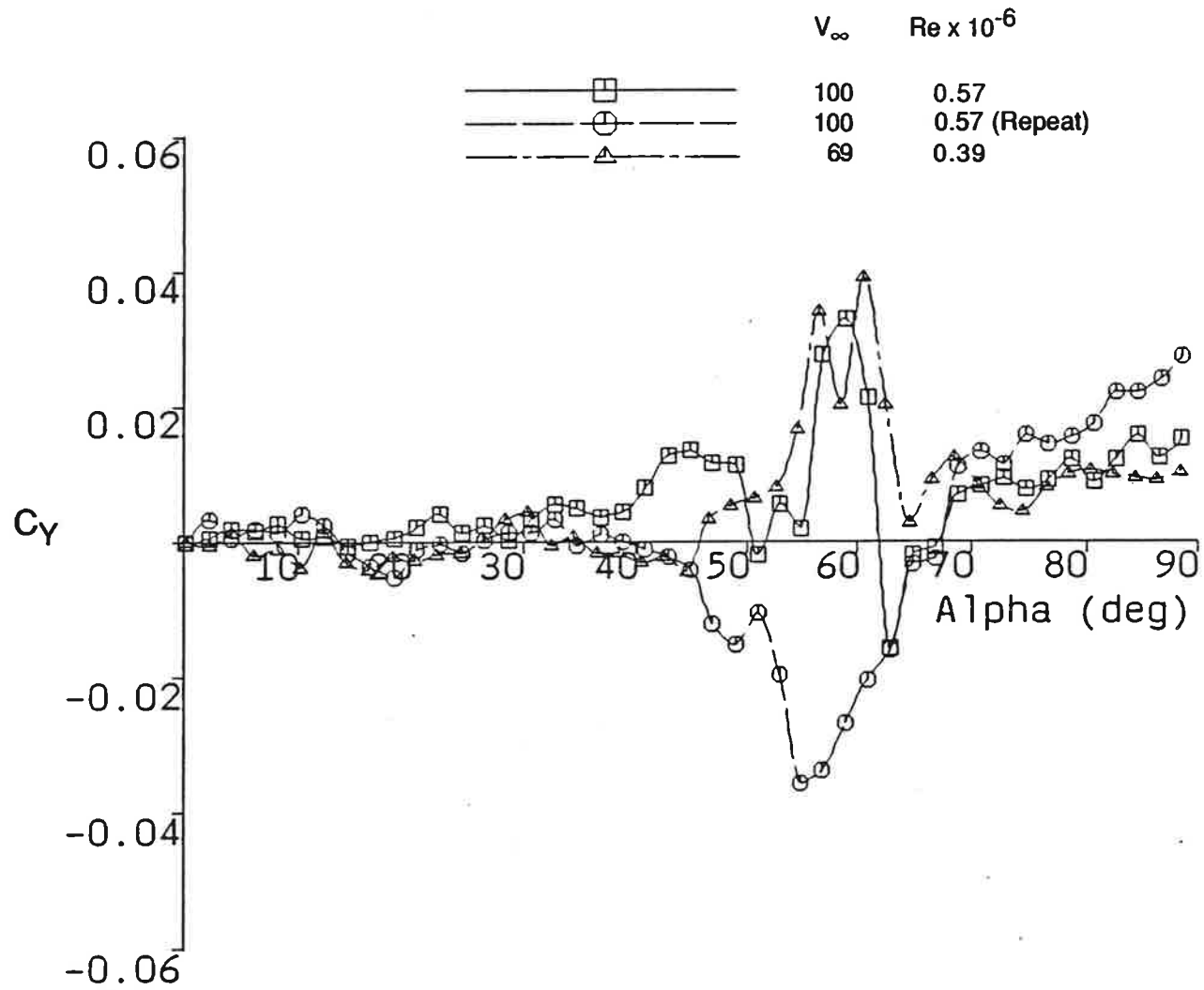


FIG. 8: SIDE FORCE AT TWO VELOCITIES

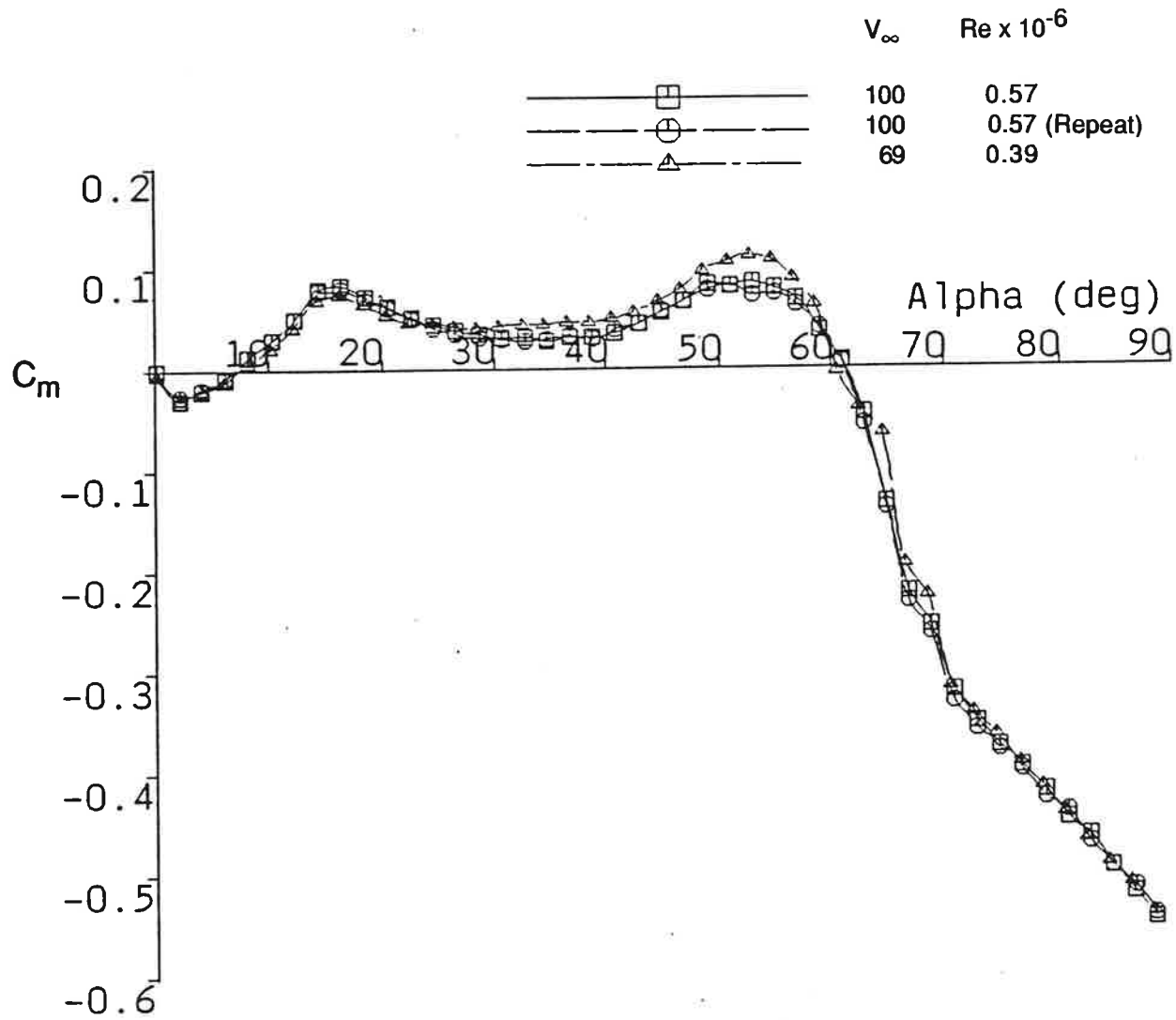


FIG. 9: PITCHING MOMENT AT TWO VELOCITIES

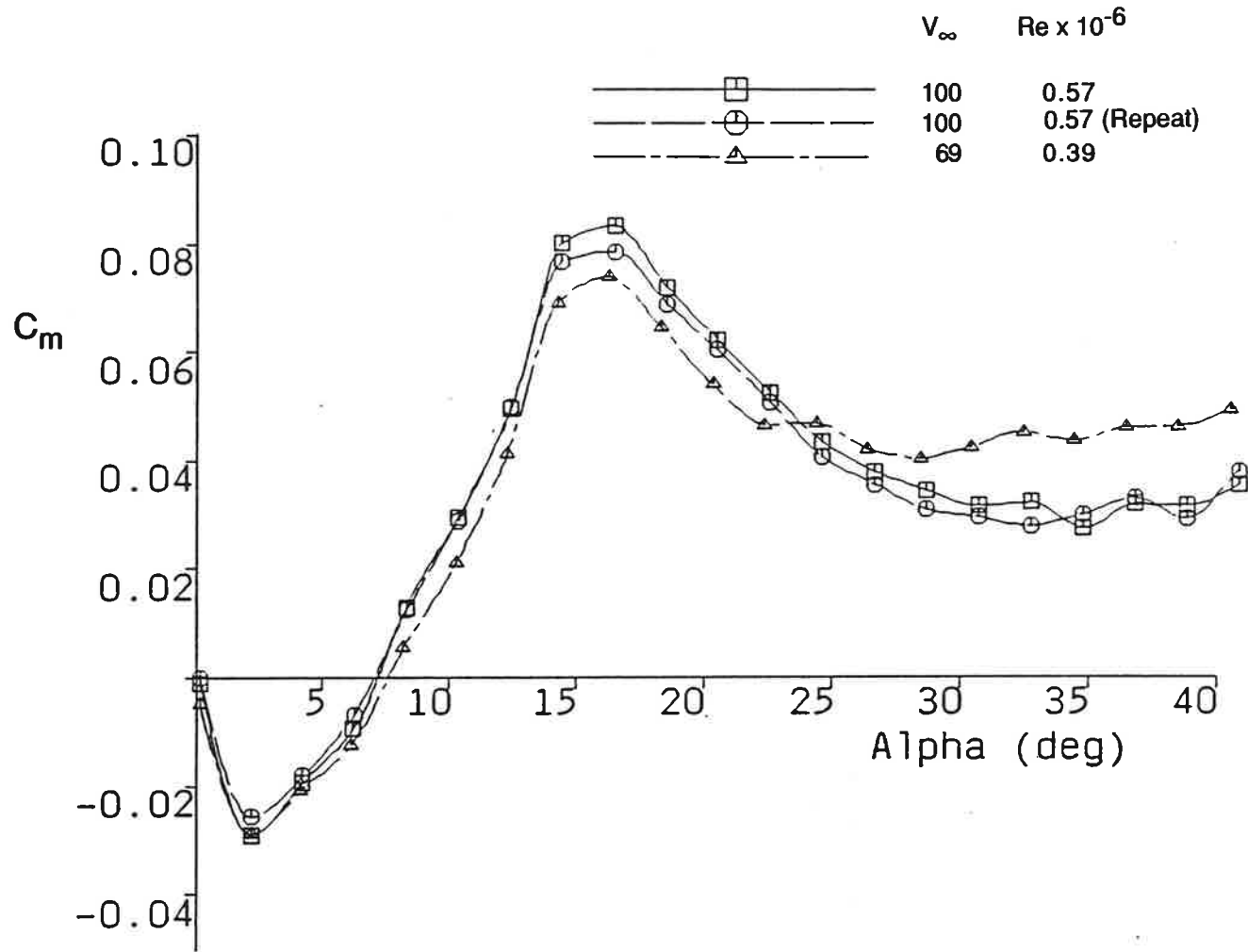


FIG. 9(a): PITCHING MOMENT AT TWO VELOCITIES

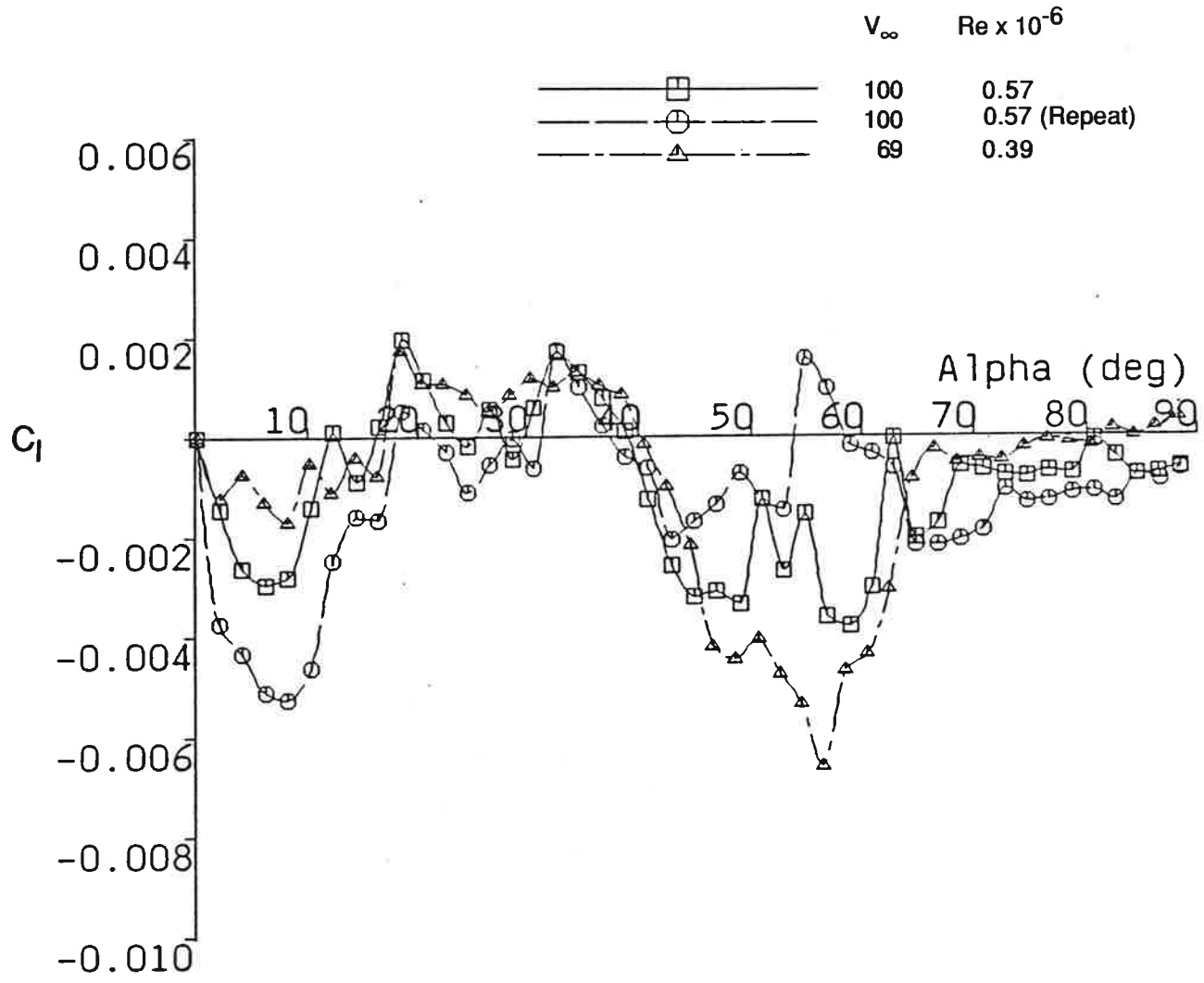


FIG. 10: ROLLING MOMENT AT TWO VELOCITIES

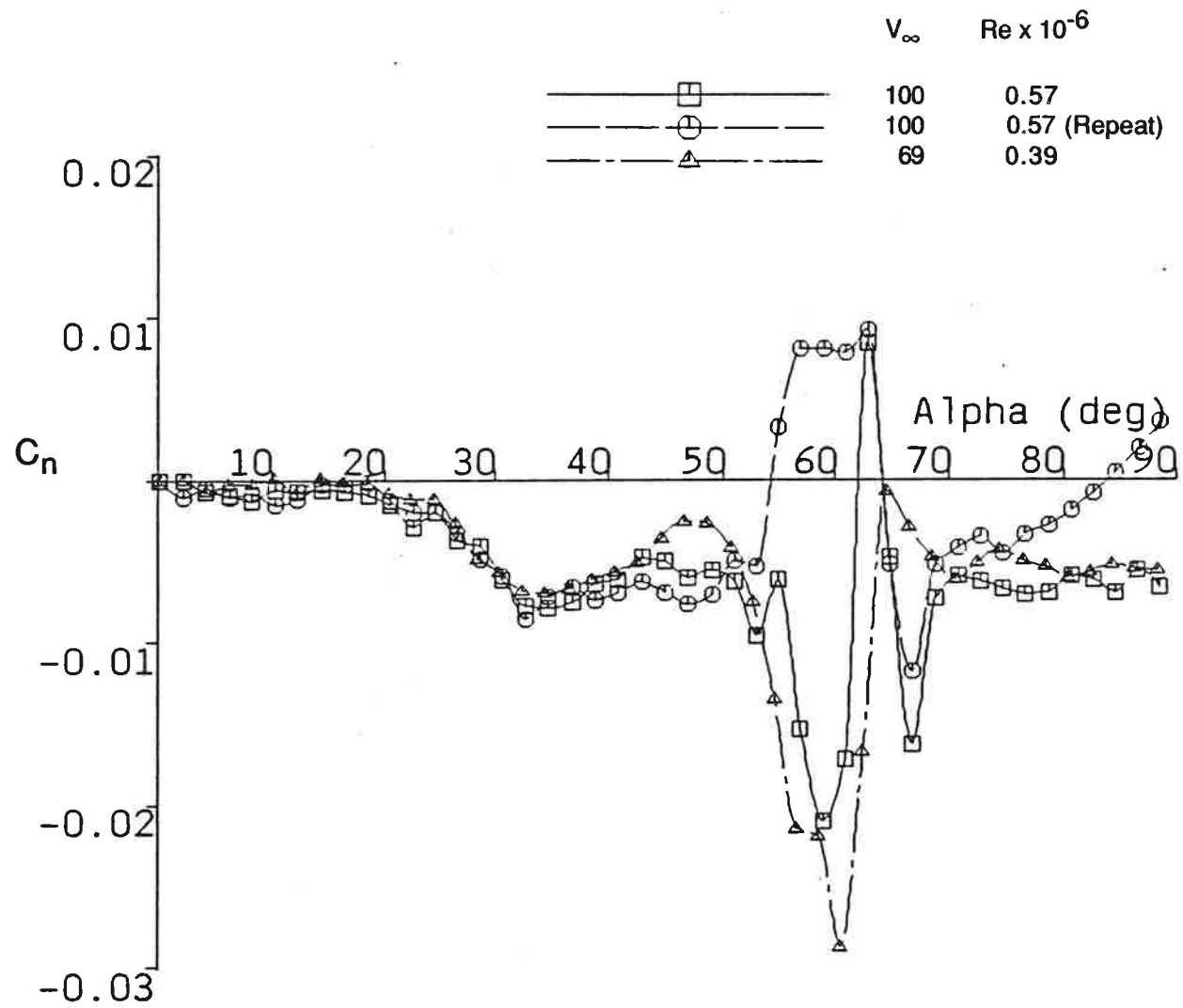


FIG. 11: YAWING MOMENT AT TWO VELOCITIES

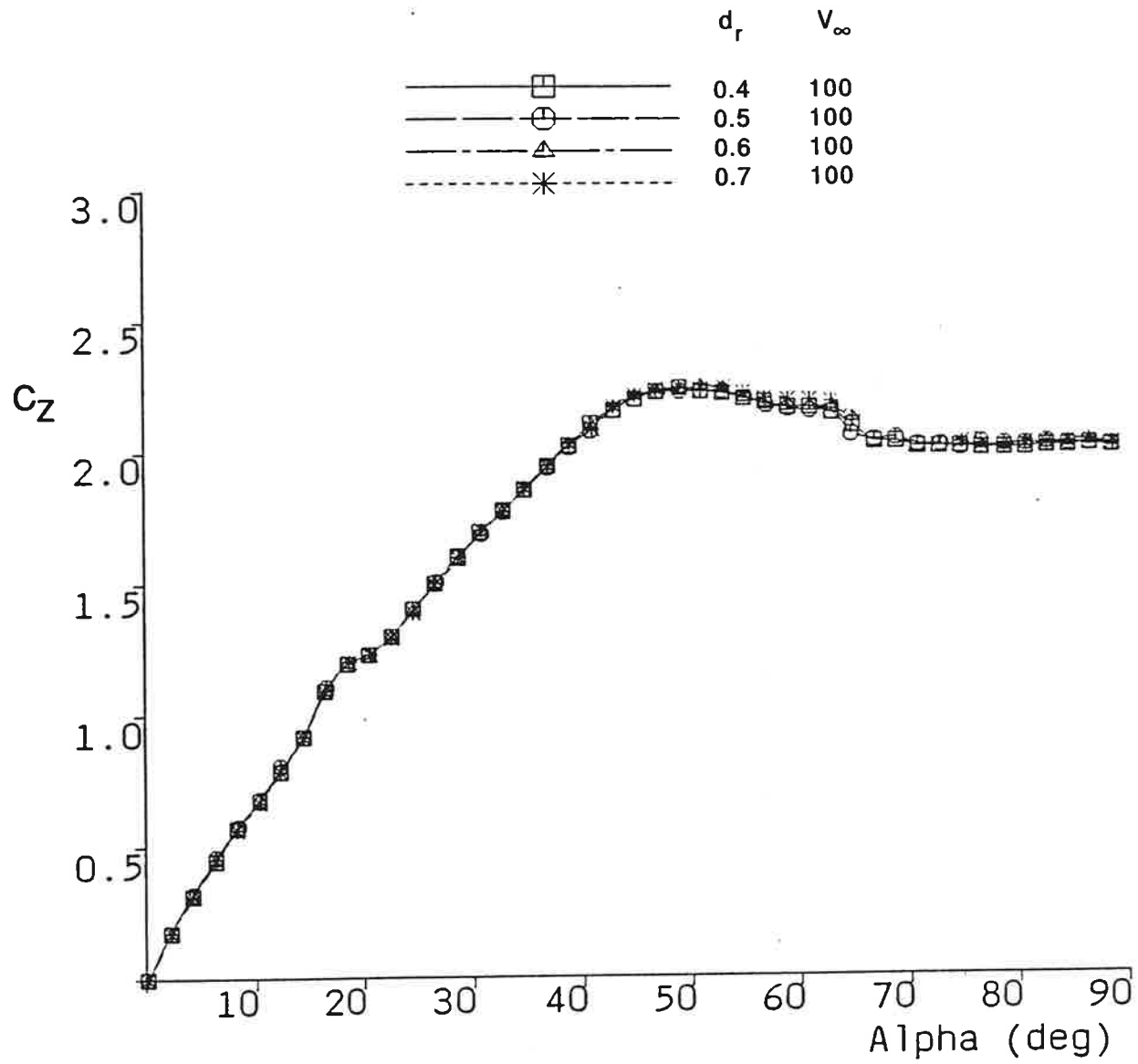


FIG. 12: STING DIAMETER EFFECT: NORMAL FORCE

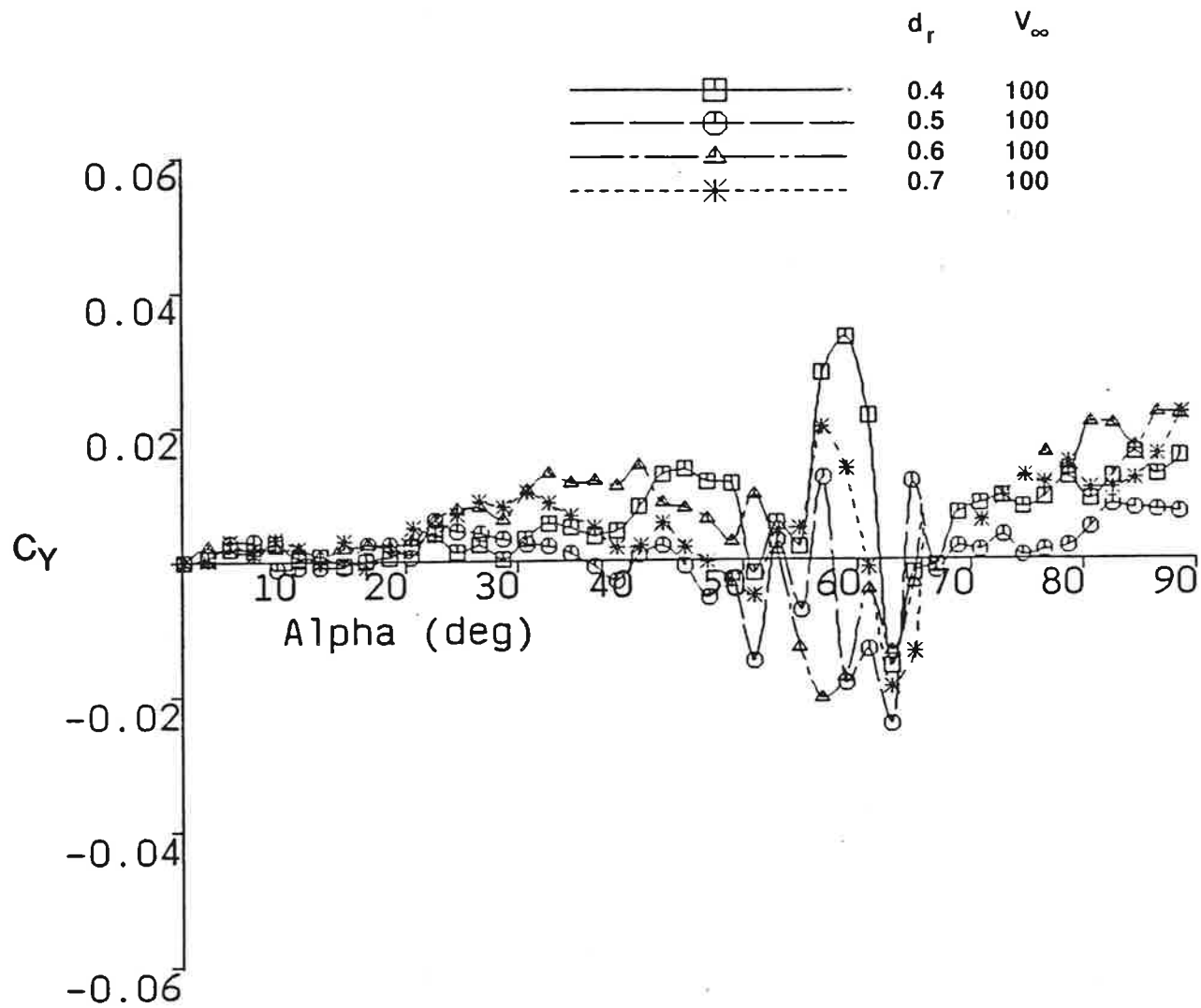


FIG. 13: STING DIAMETER EFFECT: SIDE FORCE

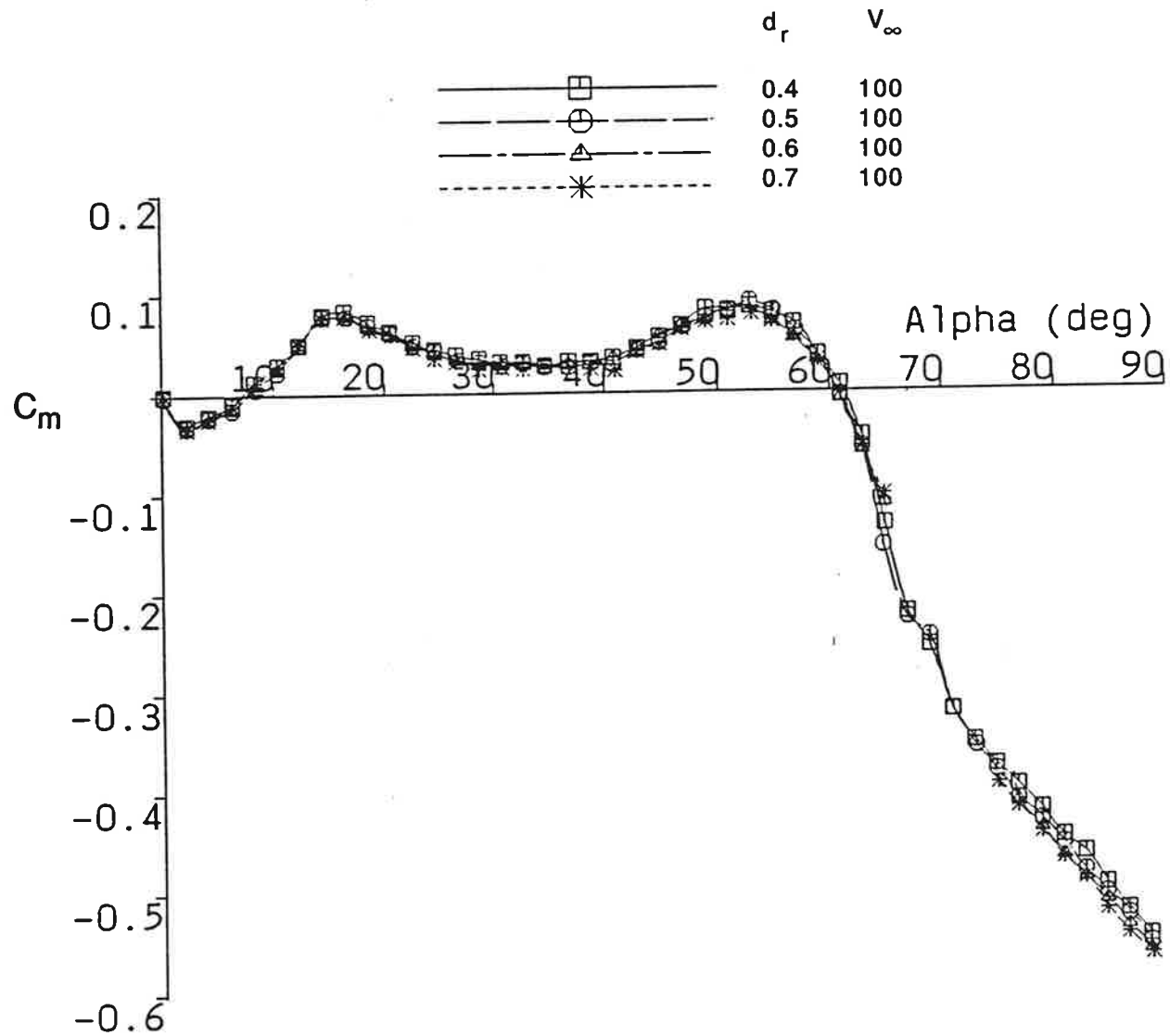


FIG. 14: STING DIAMETER EFFECT: PITCHING MOMENT

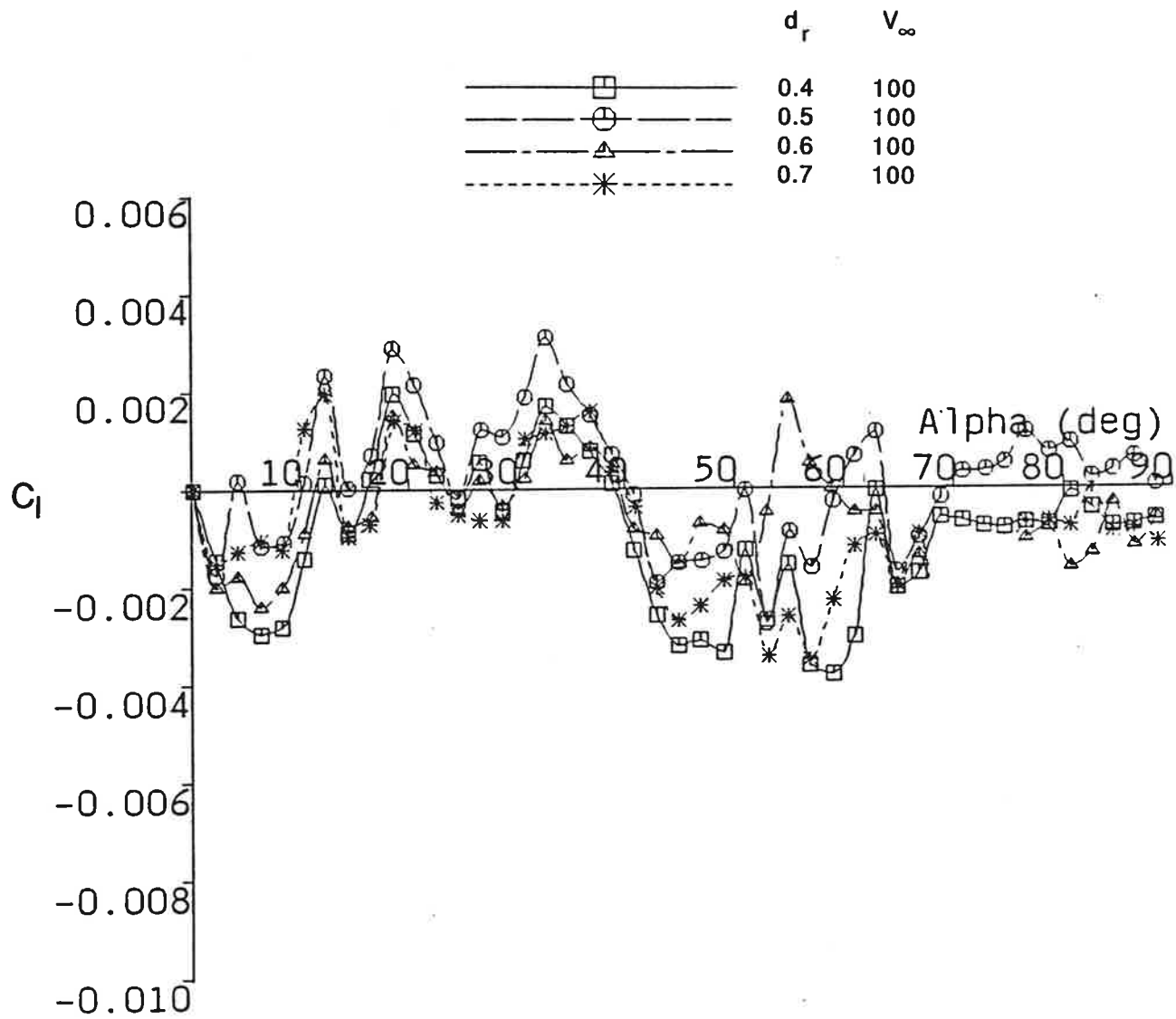


FIG. 15: STING DIAMETER EFFECT: ROLLING MOMENT

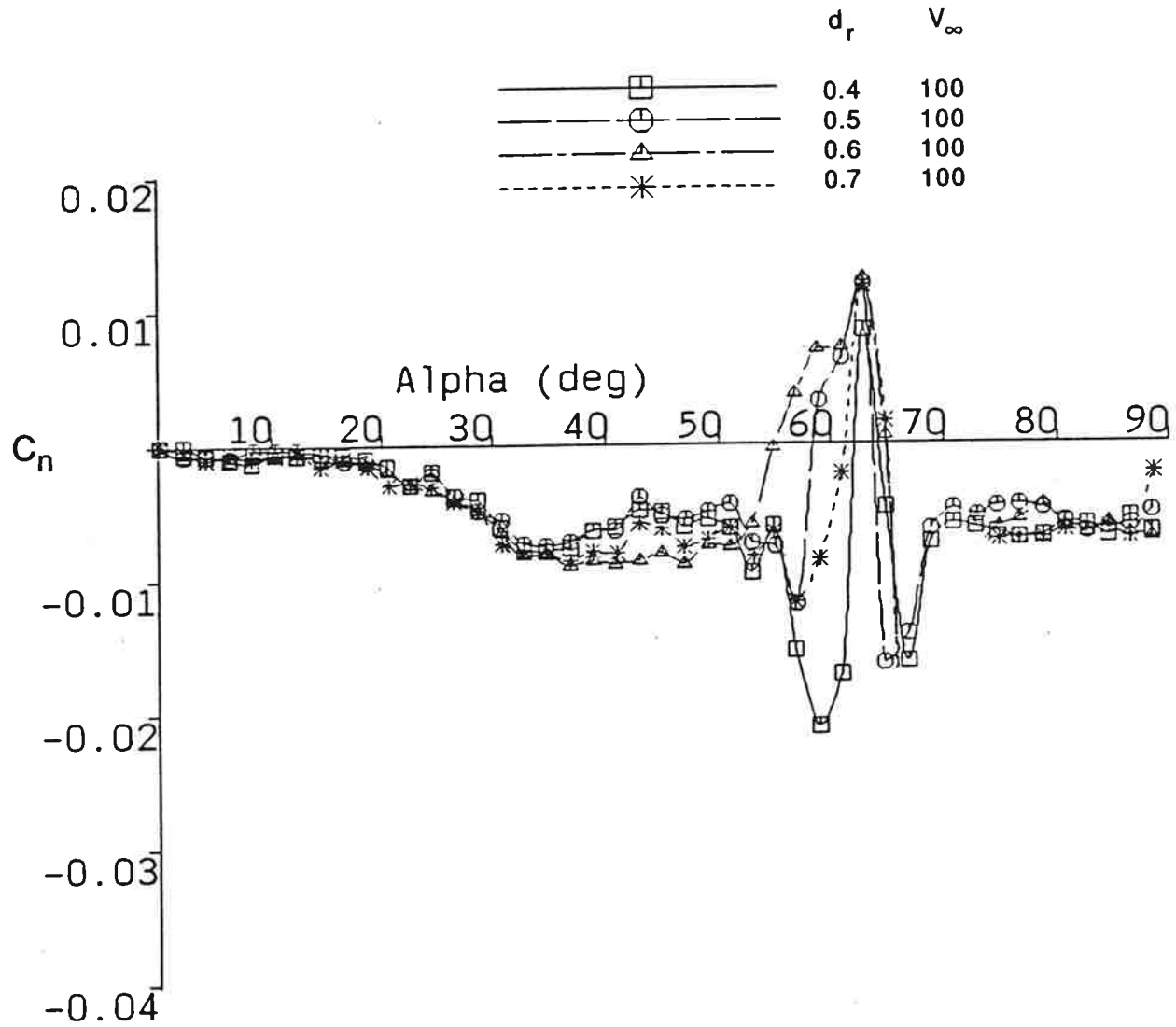


FIG. 16: STING DIAMETER EFFECT: YAWING MOMENT

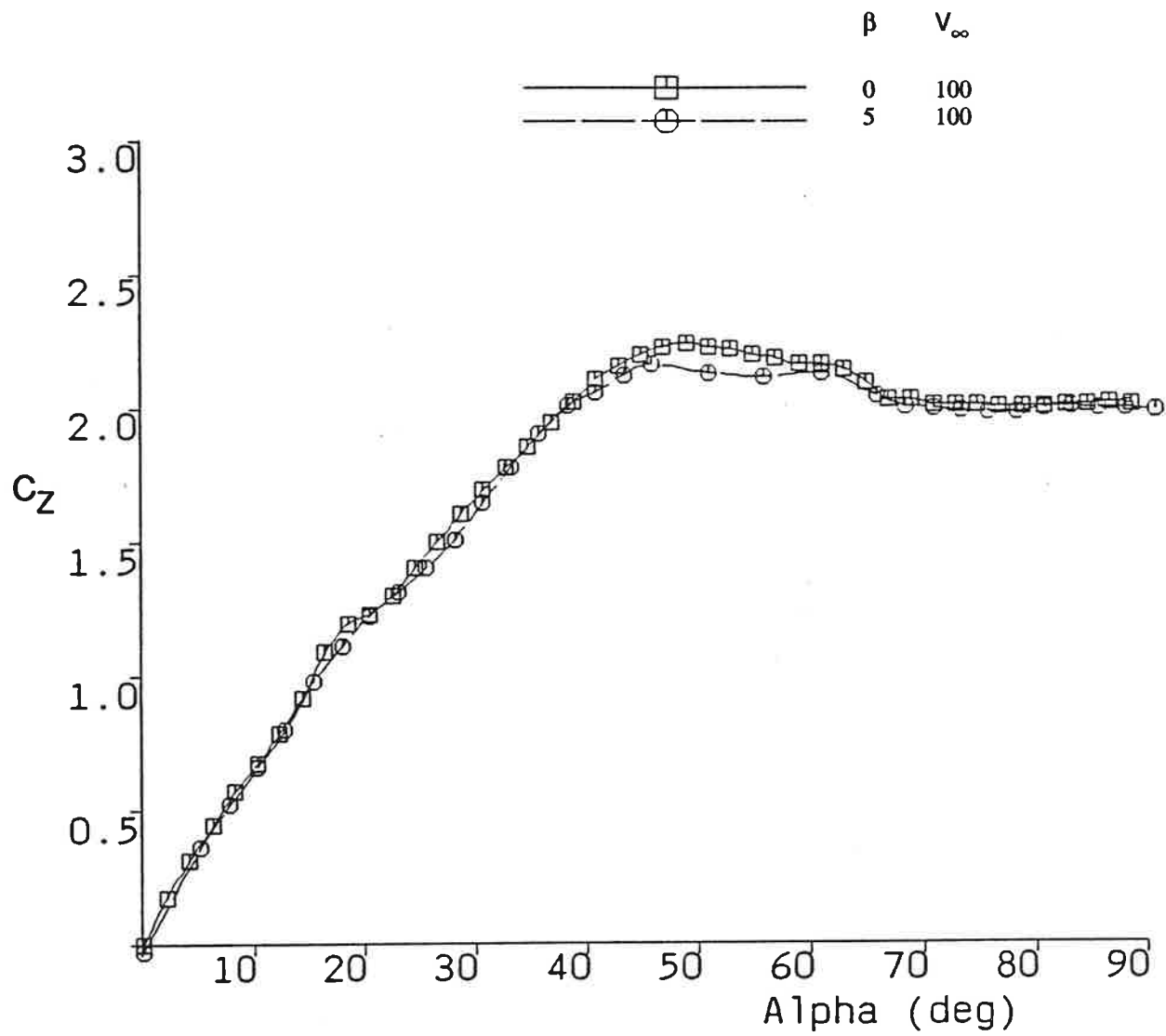


FIG. 17: SIDESLIP EFFECT ON NORMAL FORCE

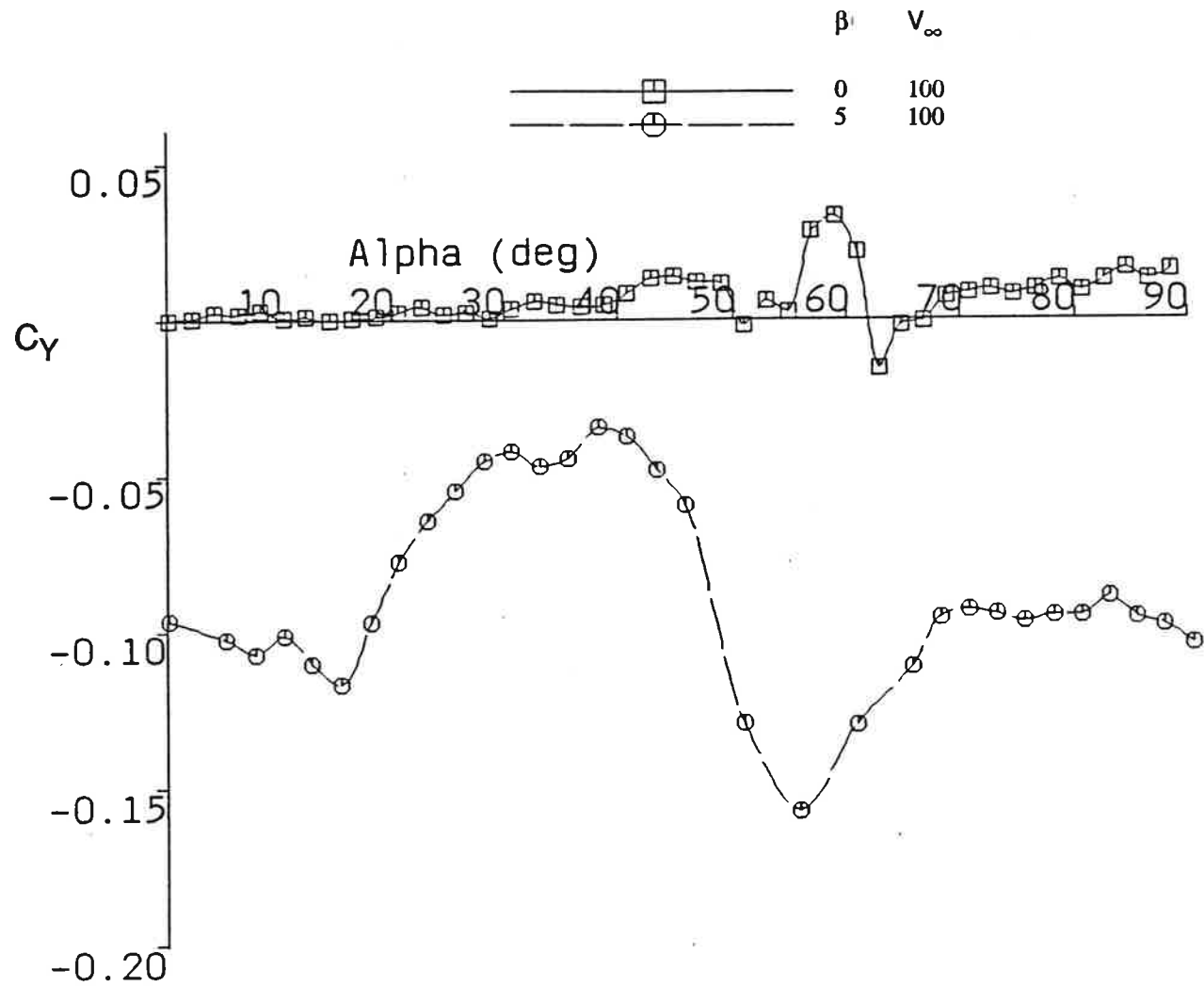


FIG. 18: SIDESLIP EFFECT ON SIDE FORCE

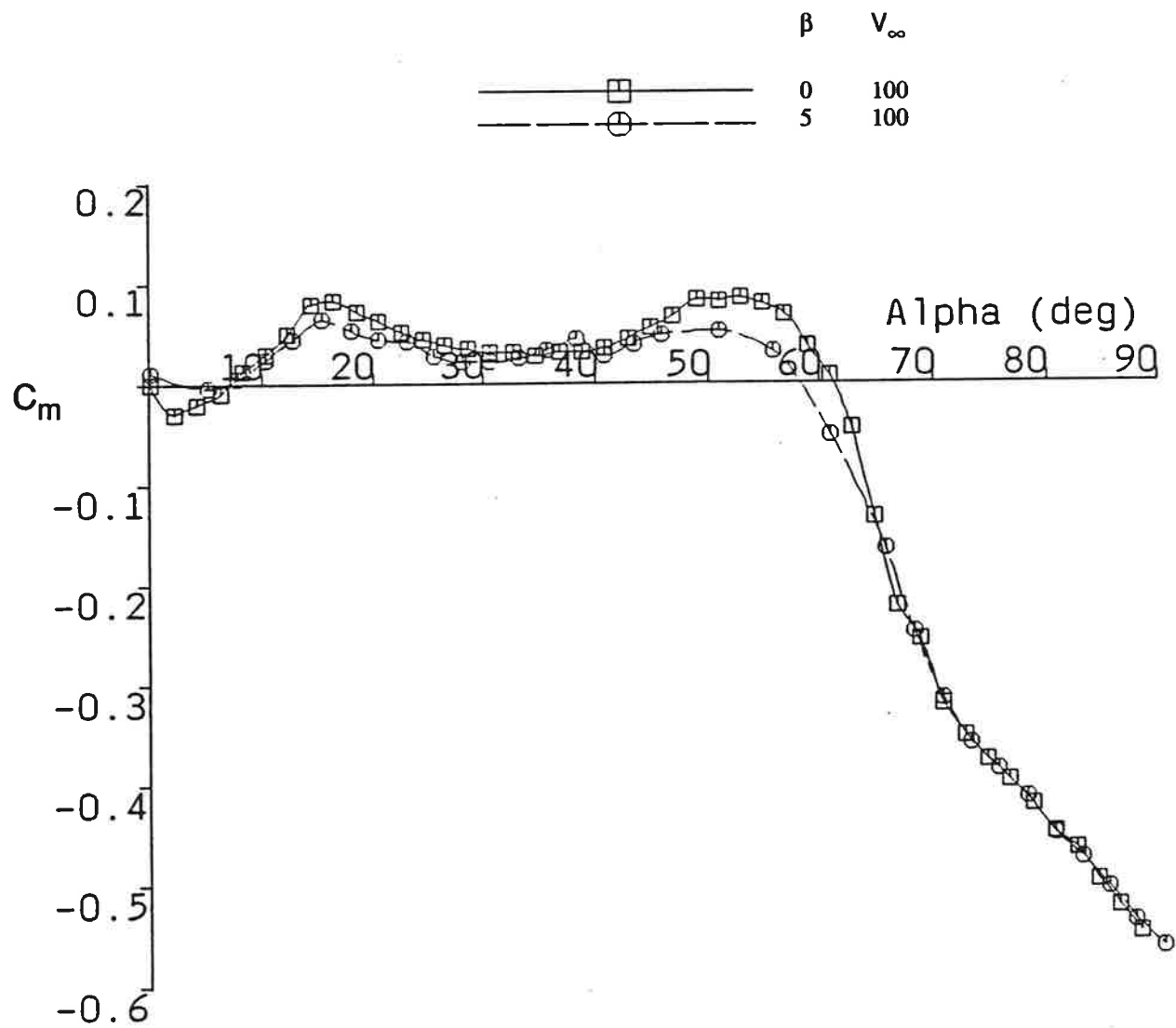


FIG. 19: SIDESLIP EFFECT ON PITCHING MOMENT

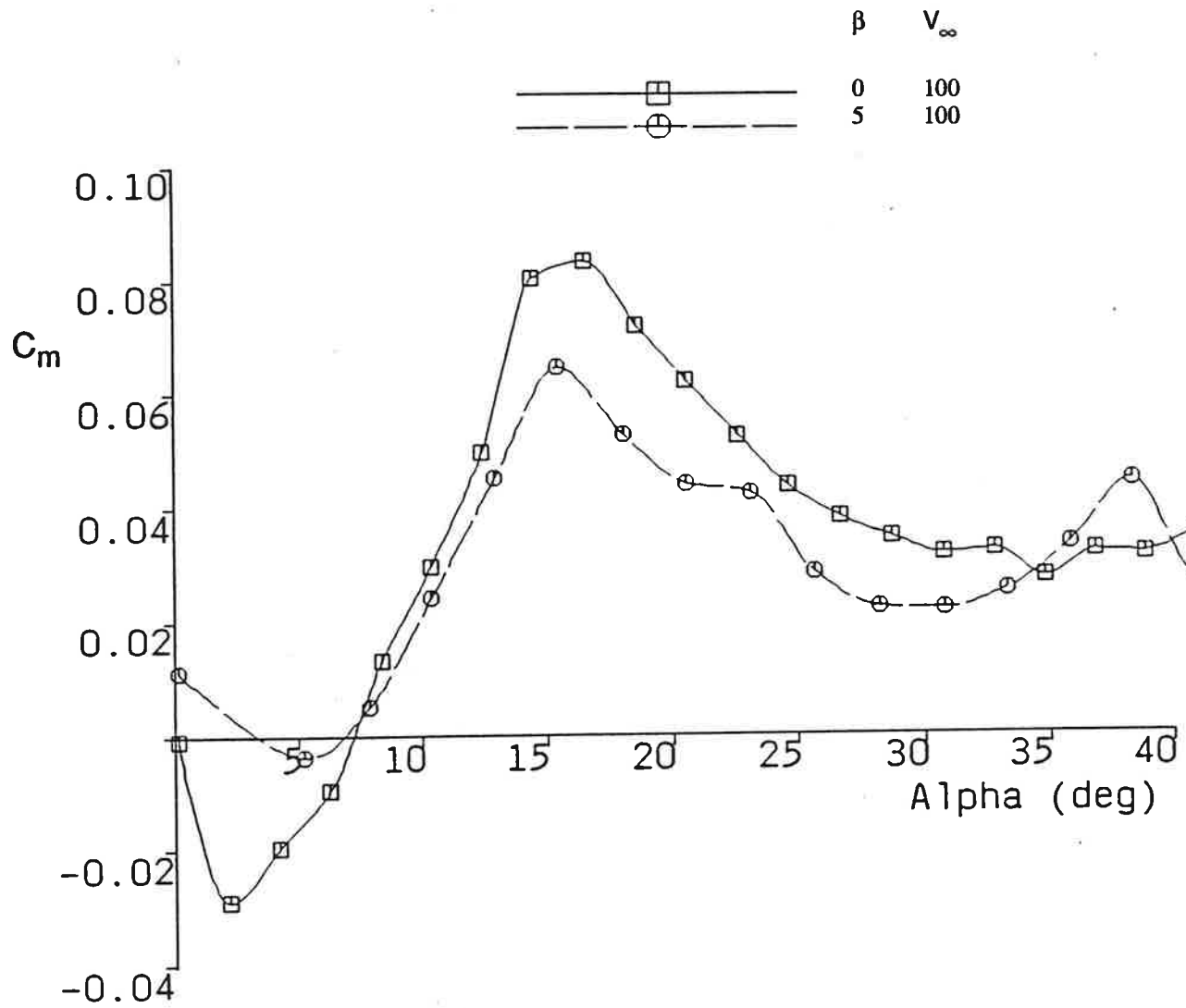


FIG. 19(a): SIDESLIP EFFECT ON PITCHING MOMENT

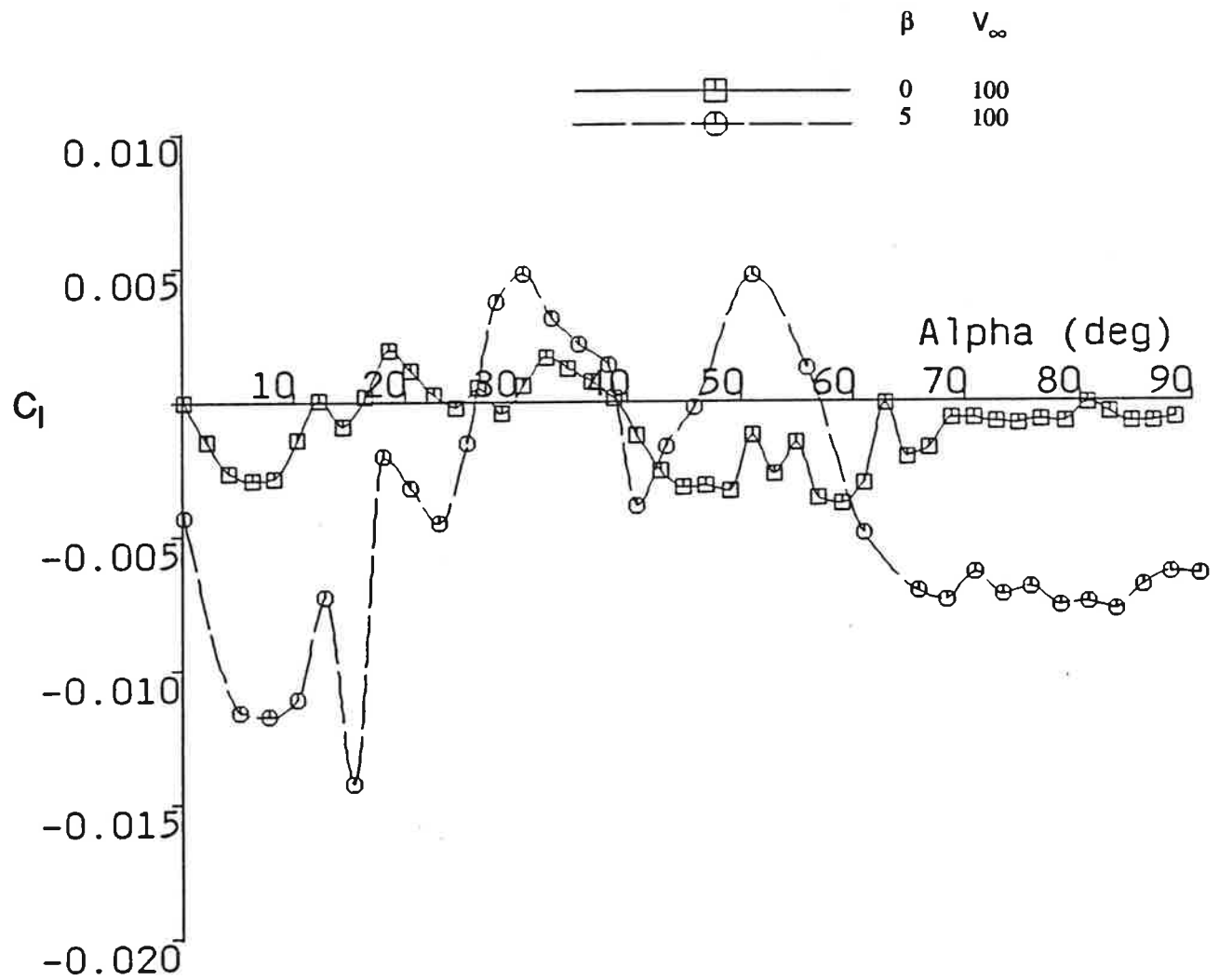


FIG. 20: SIDESLIP EFFECT ON ROLLING MOMENT

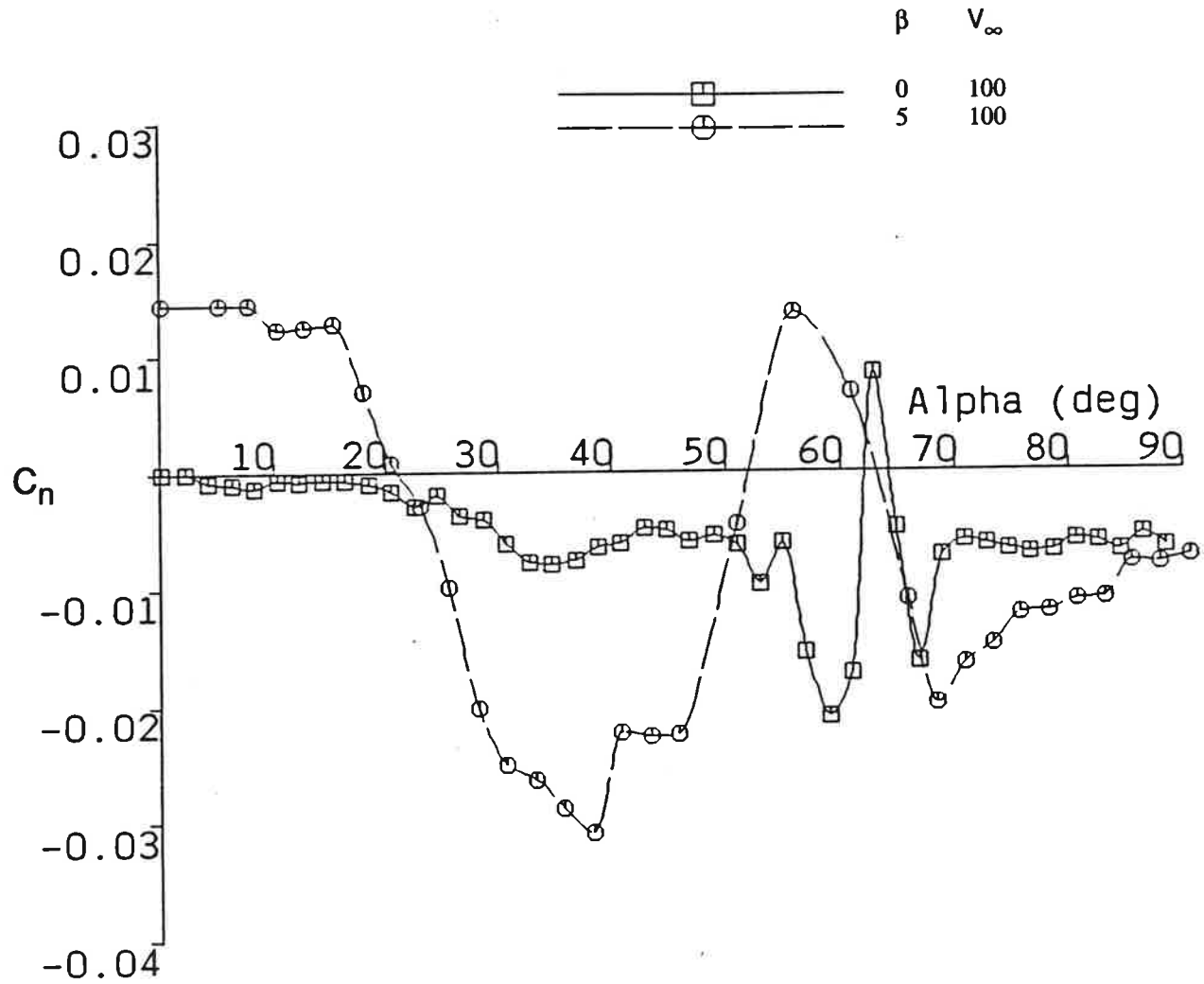


FIG. 21: SIDESLIP EFFECT ON YAWING MOMENT

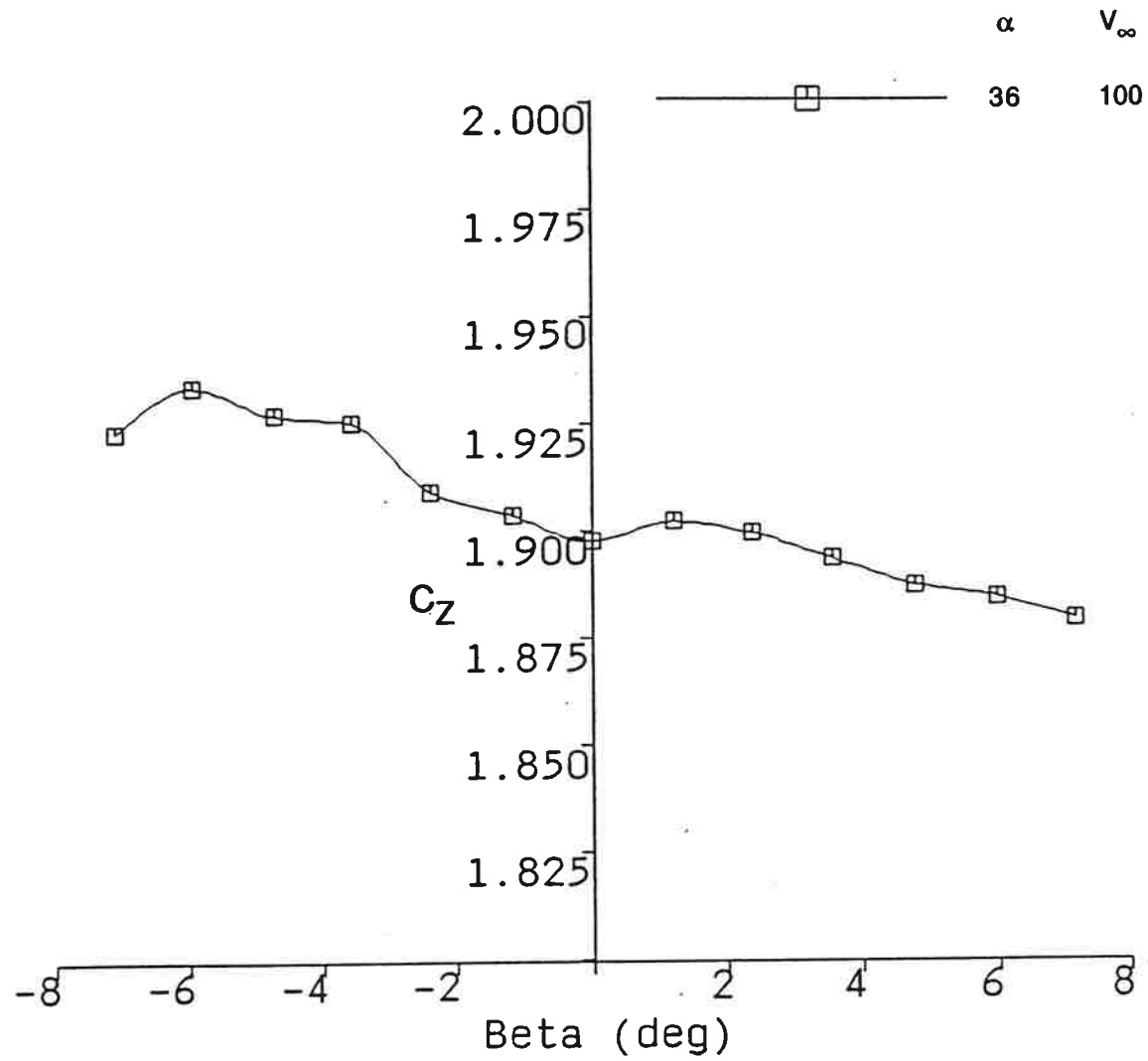


FIG. 22: NORMAL FORCE VS. SIDESLIP ANGLE

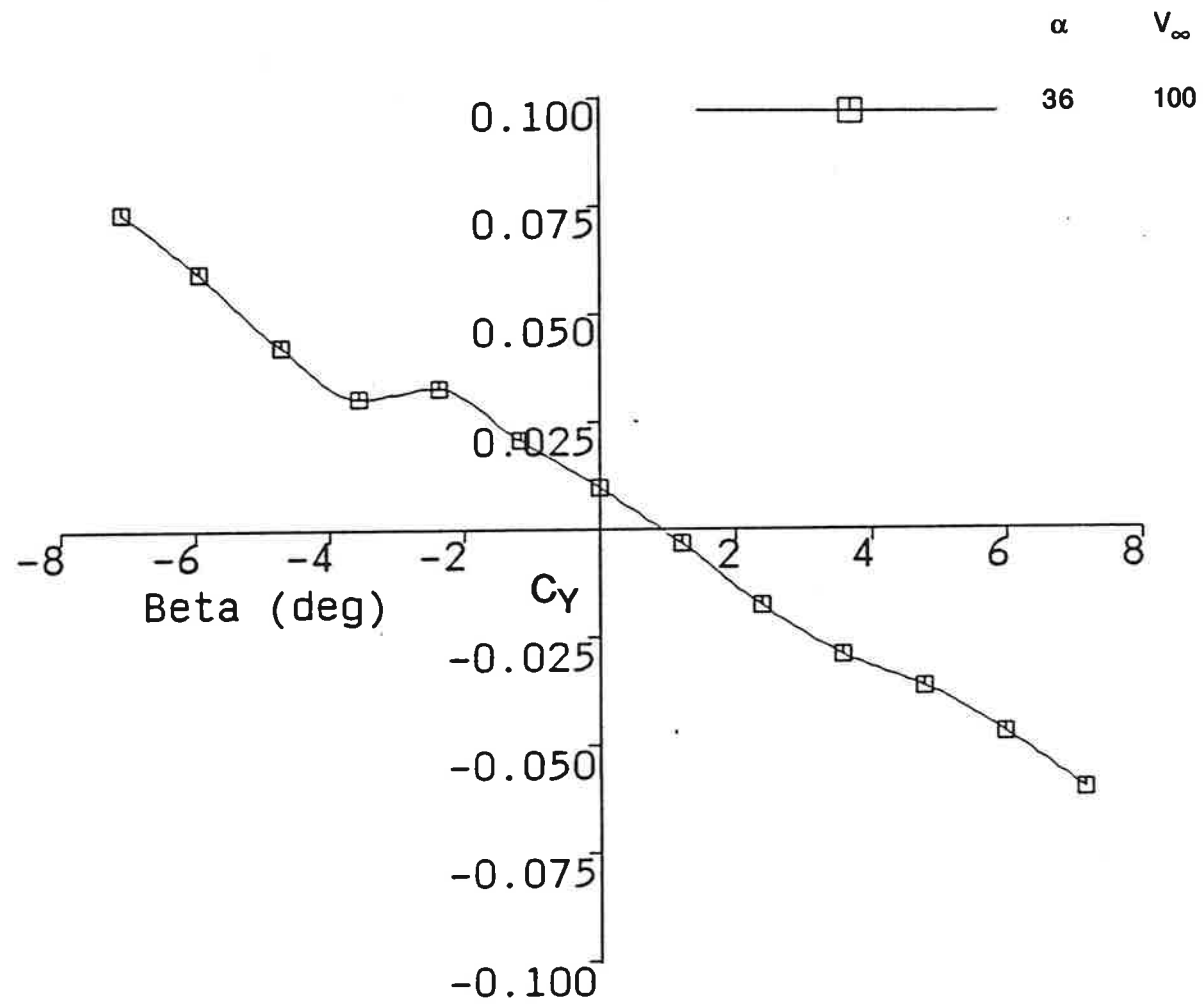


FIG. 23: SIDE FORCE VS. SIDESLIP ANGLE

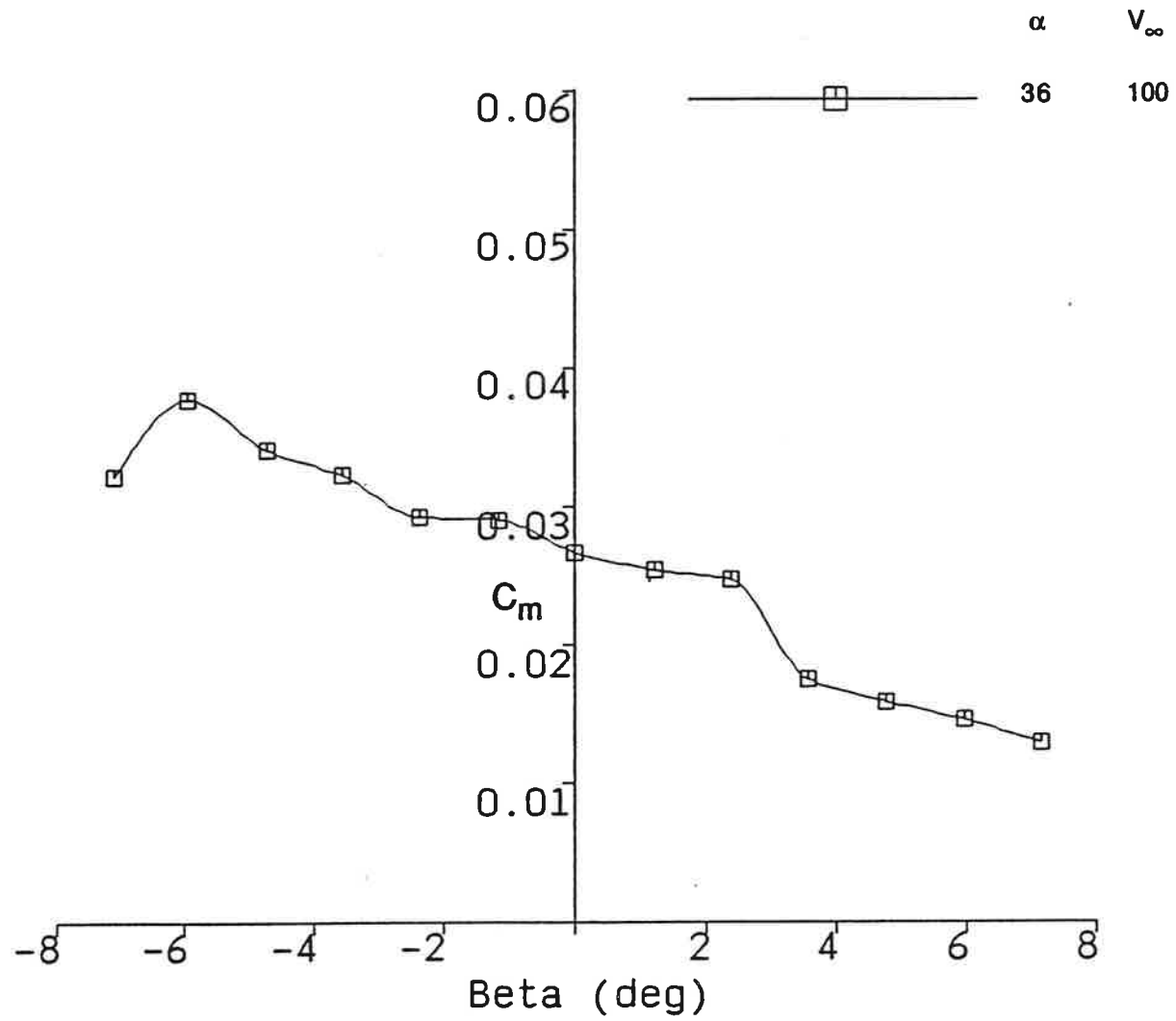


FIG. 24: PITCHING MOMENT VS. SIDESLIP ANGLE

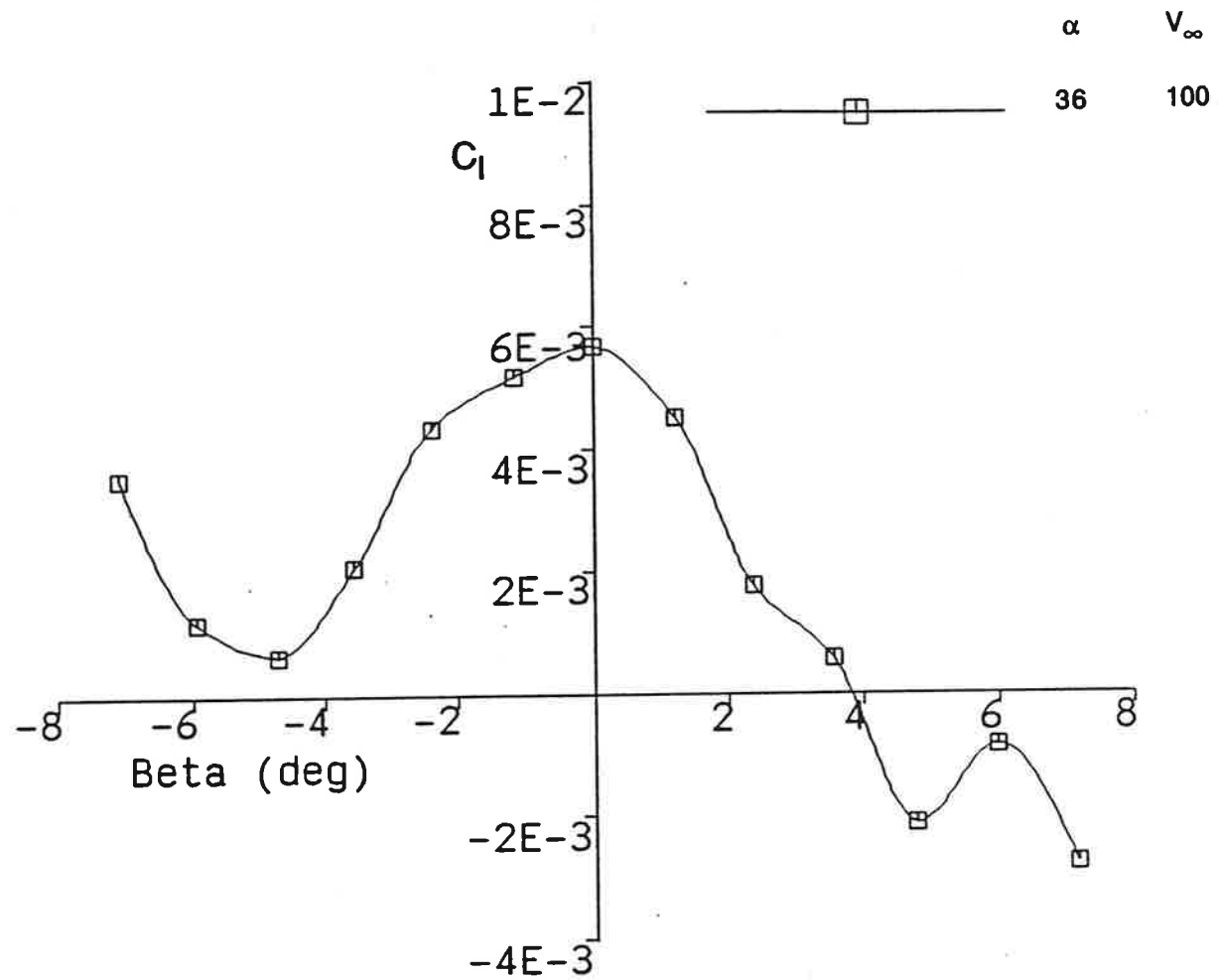


FIG. 25: ROLLING MOMENT VS. SIDESLIP ANGLE

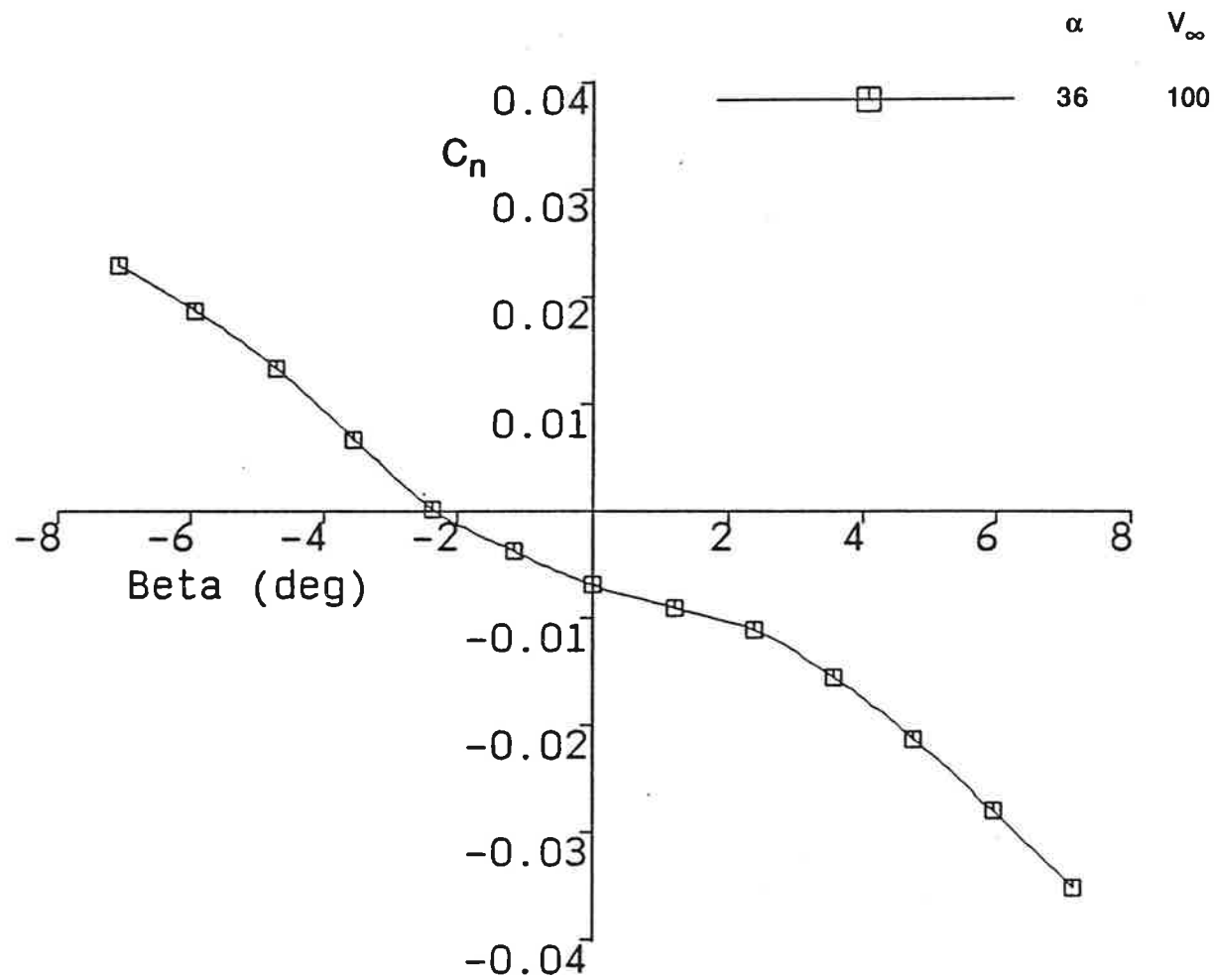


FIG. 26: YAWING MOMENT VS. SIDESLIP ANGLE

